Gas slug ascent through changes in conduit diameter: Laboratory insights into a volcano-seismic source process in low-viscosity magmas

M. R. James,[1] S. J. Lane,[1] and B. A. Chouet[2]

Received 5 March 2005; revised 23 November 2005; accepted 2 February 2006; published 6 May 2006.

[1] Seismic signals generated during the flow and degassing of low-viscosity magmas include long-period (LP) and very-long-period (VLP) events, whose sources are often attributed to dynamic fluid processes within the conduit. We present the results of laboratory experiments designed to investigate whether the passage of a gas slug through regions of changing conduit diameter could act as a suitable source mechanism. A vertical, liquid-filled glass tube featuring a concentric diameter change was used to provide canonical insights into potentially deep or shallow seismic sources. As gas slugs ascend the tube, we observe systematic pressure changes varying with slug size, liquid depth, tube diameter, and liquid viscosity. Gas slugs undergoing an abrupt flow pattern change upon entering a section of significantly increased tube diameter induce a transient pressure decrease in and above the flare and an associated pressure increase below it, which stimulates acoustic and inertial resonant oscillations. When the liquid flow is not dominantly controlled by viscosity, net vertical forces on the apparatus are also detected. The net force is a function of the magnitude of the pressure transients generated and the tube geometry, which dictates where, and hence when, the traveling pressure pulses can couple into the tube. In contrast to interpretations of related volcano-seismic data, where a single downward force is assumed to result from an upward acceleration of the center of mass in the conduit, our experiments suggest that significant downward forces can result from the rapid deceleration of relatively small volumes of downward-moving liquid.

Citation: James, M. R., S. J. Lane, and B. A. Chouet (2006), Gas slug ascent through changes in conduit diameter: Laboratory insights into a volcano-seismic source process in low-viscosity magmas, *J. Geophys. Res.*, *111*, B05201, doi:10.1029/2005JB003718.

1. Introduction

[2] The continuously improving quality of seismic data recorded at volcanoes has allowed increasingly sophisticated analytical techniques to be employed. In particular, robust source-time functions have been derived for very-long-period (VLP, 2 to 100 s) events at Stromboli [*Chouet et al.*, 2003], and Popocatépetl [*Chouet et al.*, 2005], and for long-period (LP, 0.2 to 2 s) events in hydrothermal systems [*Kumagai et al.*, 2002]. Source-time functions representing time-varying moment-tensor and single-force components allow an estimation of the fluid pressure and momentum changes that appear to be responsible for these events. Our understanding of the underlying physical fluid flow processes, however, remains poor. To develop the full potential of quantitative volcano seismology, links are required between known flow processes and the resulting pressure and momentum changes produced. In the case of magmas, the occurrence of steep viscosity gradients and non-Newtonian effects complicate the scaling of natural processes to the laboratory scale. However, low-viscosity magmatic systems, for example Stromboli, can be approximated by Newtonian behavior and scaling is considerably simpler. The experiments presented in this study use Newtonian liquids to investigate low-viscosity magmatic systems.

[3] Many LP and VLP seismic events are believed to be the result of movement of low-viscosity liquid induced by the formation and ascent of gas slugs, culminating in Strombolian or similar-style eruptions [*Neuberg et al.*, 1994; *Ohminato et al.*, 1998; *Rowe et al.*, 1998; *Kirchdörfer*, 1999; *Rowe et al.*, 2000; *Aster et al.*, 2003; *Chouet et al.*, 2003]. *Ripepe and Gordeev* [1999] suggested that forced coalescence of bubbles at a physical barrier (e.g., a severe constriction in the conduit) must occur in order to explain the magnitude of their volcanic tremor data from Stromboli. They considered the viscoelastic response of bubbly magma when deriving repeat periods for seismic and acoustic events, and calculated pressure variations of $\sim$10 kPa purely on the grounds of changes in static head. The source mechanisms derived by *Chouet et al.* [2003] from inversions of the VLP waveforms from Strombolian explosions point to a pressure increase on the order of 10 MPa, and their analysis of bubble dynamics suggests that only liquid inertia during a period of rapid gas phase

[1]Department of Environmental Science, Lancaster University, Lancaster, UK.
[2]U.S. Geological Survey, Menlo Park, California, USA.

0148-0227/06/2005JB003718$09.00

expansion is capable of producing a superstatic pressure of this magnitude. A corresponding downward single force of ~100 MN is interpreted as the result of an upward acceleration of the magma column on top of an expanding gas slug. A superstatic slug pressure of 10 MPa at depth was also invoked by *Vergniolle* [1998] to explain acoustic data from Stromboli. However, no mechanism has yet been proposed to elucidate the origin of a superstatic pressure of such magnitude. Thus considerable uncertainty remains in the processes responsible for LP and VLP events during slug flow, and the relative importance of static, steady dynamic, and transient fluid dynamic effects is unknown. VLP events also occur through a variety of other mechanisms [e.g., *Chouet et al.*, 2005], but we do not address these here.

[4] Previous laboratory experiments aimed at the study of acoustic sources applicable to low-viscosity magmatic systems have generally considered only smooth, straight tubes [*Vergniolle et al.*, 1996; *James et al.*, 2004]. This geometry is appropriate for the shallowest levels in a volcano, where thermal considerations control the shape of long-lived conduits [e.g., *Bruce and Huppert*, 1989], and such geometry also provides benchmark data from which processes occurring within more complicated systems can be explored and understood. At greater depths, where conduit behavior becomes increasingly controlled by the local stress field and the presence of fracture planes, magma pathways are more likely to be better represented by individual, or arrays of, dikes. This, along with the fact that edifices are generally composed of highly inhomogeneous materials, strongly suggests that changes in conduit size, shape and angle are likely [e.g., *Chouet et al.*, 2005; *Gutmundsson*, 2005]. *Seyfried and Freundt* [2000] investigated the effect of rough-walled conduits by carrying out experiments with concurrent gas and liquid flows through a vertical tube containing obstacles. Their results suggest that the presence of obstacles is less important than slug coalescence processes for generating pressure changes. However, the underlying pressure changes induced by the ascent of individual slugs, or by slugs rising within a stationary liquid phase, were not considered. Although engineering-oriented research has generated a large body of work on slug flow [e.g., *Fabre and Liné*, 1992; *Taha and Cui*, 2006, and references therein] the authors are unaware of any previous literature on the ascent of gas slugs through sudden changes in tube diameter. Other work carried out on conduits displaying sudden expansions or contractions with single-fluid, bubbly or foam flows [*Aloui et al.*, 1999; *Deshpande and Barigou*, 2001; *Poole and Escudier*, 2003], particle-laden flows [*Sommerfeld et al.*, 1992; *Founti et al.*, 1999] and liquid displacement by gas injection [*Dimakopoulos and Tsamopoulos*, 2003a, 2003b] has targeted variations of bulk fluid properties or time-averaged pressure changes. In the present study, we further develop previous work by *James et al.* [2004] to investigate the dynamics of a single slug ascending in a stationary liquid within regions of changing tube geometry. To limit experimental complexity but capture the essential physics, we restrict our attention to a vertical tube with circular cross section. Our objective is to describe accurately the processes that occur during the passage of a gas slug through a change in tube diameter. This is achieved through detailed recordings of pressure and force data, and through observations of how these data vary with parameters such as liquid viscosity and slug size.

2. Methods

2.1. Experimental Scaling

[5] The slug flow regime describes two-phase flow where large bubbles with diameters approaching that of a confining pipe rise within a continuous liquid phase. We adopt the terminology commonly used in the volcanology literature [*Jaupart and Vergniolle*, 1989; *Seyfried and Freundt*, 2000; *Ripepe et al.*, 2001; *James et al.*, 2004] and by *Clift et al.* [1978], in which the gas phase is referred to as the slug. The laboratory experiments can be compared with low-viscosity magmatic systems using three dimensionless parameters relevant to gas slugs ascending buoyantly in liquid-filled tubes [*White and Beardmore*, 1962; *Clift et al.*, 1978]. These are the Froude number (balance of inertia and gravity)

$$Fr = \frac{U_o}{\sqrt{gD}}, \tag{1}$$

Morton number (balance of viscosity and surface tension)

$$Mo = \frac{g\mu^4}{\rho\sigma^3}, \tag{2}$$

and Eötvös number (balance of gravity and surface tension)

$$Eo = \frac{\rho g D^2}{\sigma}. \tag{3}$$

We also consider a dimensionless inverse viscosity

$$N_f = \left(\frac{Eo^3}{Mo}\right)^{\frac{1}{4}} = \frac{\rho D^{\frac{3}{2}} g^{\frac{1}{2}}}{\mu}, \tag{4}$$

where U_o represents the terminal ascent velocity of the slug, g is the acceleration due to gravity, D is the internal diameter of the tube, and μ, ρ and σ are the viscosity, density, and surface tension of the liquid, respectively.

[6] In vertical conduit low-viscosity magmatic systems, the typical ranges of these parameters are $0.1 < Fr < 0.35$, $10^5 < Eo < 10^7$, $10^5 < Mo < 10^{10}$ and $16 < N_f < 5000$, assuming $50 < \mu < 500$ Pa s, $\rho = 2600$ kg m^{-3} and $\sigma = 0.4$ N m^{-1} for basalt, and $1 < D < 10$ m for the conduit [*Seyfried and Freundt*, 2000]. These ranges indicate that gas slugs ascend within inertial and transitional regimes, in which the slug velocity is a function of both slug buoyancy and liquid viscosity [*White and Beardmore*, 1962]. In the experiments described here, $0.038 \leq D \leq 0.08$ m, $0.006 < U_0 < 0.3$ m s^{-1}, $0.001 < \mu < 30$ Pa s, $1000 \leq \rho \leq 1340$ kg m^{-3} and $\sigma \approx 0.07$ N m^{-1}, with associated dimensionless number ranges of $0.01 < Fr < 0.35$, $200 < Eo < 1200$, $10^{-11} < Mo < 10^7$, and $1 < N_f < 30000$. As the diameter of our laboratory-scale pipe dictates a much smaller Eötvös number than found in low-viscosity magmatic systems, surface effects will be relatively enhanced in our experiments. However, for $Eo > 100$, surface tension plays little role in slug ascent so that this difference should not represent a controlling factor [*Wallis*, 1969]. The inverse viscosity can be used to

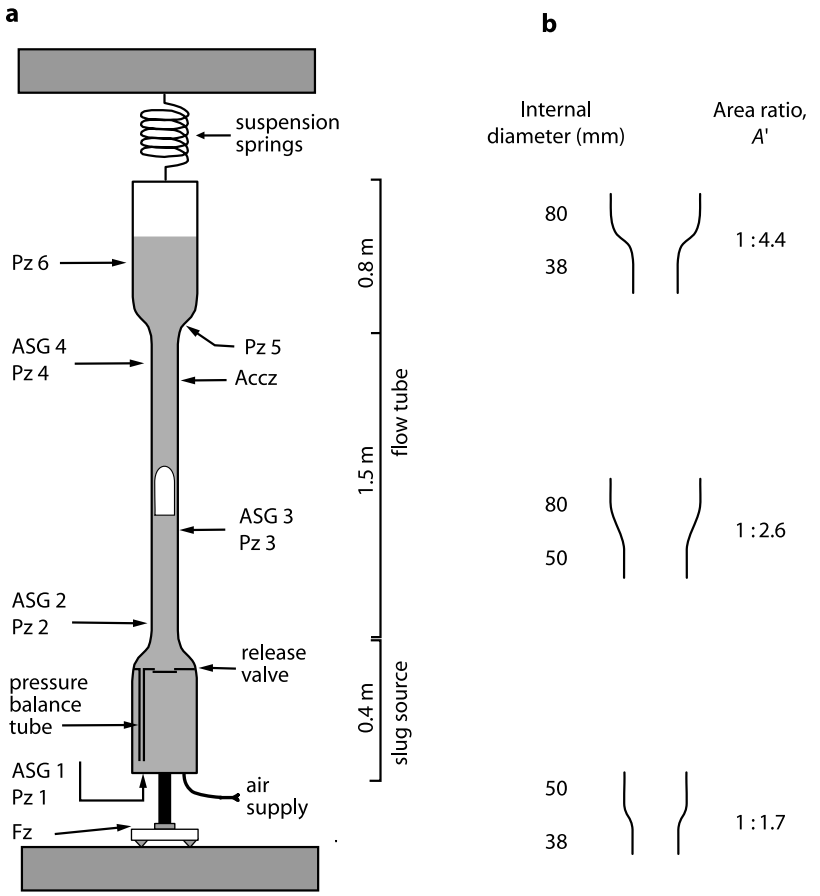

Figure 1. Experimental apparatus. (a) The equipment consists of a liquid-filled glass flow tube mounted on a gas-slug source mechanism and suspended from springs attached to the ceiling. Piezo (Pz) and active strain gauge (ASG) pressure sensors, along with an accelerometer (Accz), are mounted at the positions indicated on the tube and source mechanism. The base of the apparatus rests on a force sensor (Fz), which is used to detect vertical motion of the equipment. Air is supplied to the base of the slug source, and a gas slug is released up the flow tube by opening the release valve. (b) Scaled sketches of the internal profiles of the flared sections used in the flow tube. The cross-sectional area ratio, A', and relevant tube internal diameters are indicated by each sketch.

define regimes for viscous control ($N_f < 2$) and for an inviscid approximation ($N_f > 300$) [*Fabre and Liné*, 1992]. The majority of our laboratory flows were carried out with $30 < N_f < 30000$, although a few high-viscosity runs with $1 < N_f < 3$ were also explored in order to observe results obtained under negligible inertial influence.

[7] Consideration of these dimensionless numbers indicates that our experiments cover and exceed the steady slug ascent regimes relevant to low-viscosity magmatic systems. Therefore processes observed within the laboratory should provide insights into volcanological situations. Note, however, that the dimensionless scaling used here is only applicable to steady state flows, and that an equivalent scaling framework does not exist for transient or rapidly changing parameters. Therefore care is required when applying these results to scale the transient dynamic phenomena believed responsible for some volcano-seismic signals.

2.2. Apparatus

[8] The apparatus consists of an open-ended flow tube mounted on top of a gas slug source mechanism. The complete system is suspended on springs attached to a rigid concrete ceiling (Figure 1a). The flow tube is made of a circular cross section borosilicate glass pipe with pressure sensors mounted flush with the inside wall. Pipe sections of different diameters are joined with short, concentric reducers (Figure 1b) to give a range of cross sectional area ratios, A'. The gas slug source mechanism is constructed from a 300-mm-long section of pipe with internal diameter of 80 mm and includes a gas release poppet valve located at the top (Figure 1a). The release valve comprises a 48-mm-diameter aperture, which is normally closed by the valve plate. Before each experiment, the slug source is charged by introducing air at the base of the tube to form a gas pocket underneath the release valve. The gas pocket is maintained at hydrostatic pressure by pressure balance tubes which allow liquid to be displaced from the source region during the charging process. A slug is formed by retracting the valve plate downward, allowing the gas pocket to rise into the flow tube. The geometry and operation of the valve are such that a simple and continuous exchange current forms a single gas slug in a highly repeatable manner with minimum transient effects. Hence as slugs approach the diameter

change regions of the flow tube, they are ascending in a stable manner with all transients associated with their release having fully decayed.

[9] Within the flow tube and slug source, two different types of pressure sensor are used, namely BOC Edwards Active Strain Gauges (ASG sensors) and PCB Piezotronic ICP quartz piezo-transducers (Pz transducers). The ASG pressure sensor has a frequency range of DC to ~1 kHz, and an absolute accuracy of ±400 Pa. The Pz transducers have a higher frequency range extending from ~10 to >100 kHz, but a less well-characterized absolute calibration. Using the two types of sensors in parallel allows the recording of both absolute and high-frequency pressure data. With the exception of data collected in the concentric reducer, on which ASG sensors could not be mounted, the pressure sensors are paired so that one sensor of each type is present at each measurement point (Figure 1a). This allows cross-checking of the two data sets within the band of overlapping frequencies, which facilitates the calibration of the Pz transducers and confirms that artefacts are not being introduced by apparatus vibrations.

[10] At the base of the slug release mechanism, a sturdy aluminum platform is used to position the apparatus onto a force sensor (Fz). The force sensor is rigidly mounted within a solid metal casing, which rests on concrete blocks. Three threaded feet under the casing allow the sensor to be raised underneath the apparatus until the sensor is under a compression of half of its full scale deflection, thereby enabling the detection of both downward- and upward-directed vertical forces. The force sensor is an S-100 thin film load cell (Strain Measurement Devices, Ltd.) with a 50 N range, amplified by an AMP-M10K full bridge amplifier (Techni Measure). This transducer acts like a stiff spring (a bending beam with spring constant of $\sim 2 \times 10^5$ N m^{-1}) and, in association with the mass of the apparatus (~30 kg), the system has a natural oscillation frequency of ~13 Hz.

[11] It is usually recommended that the analysis of force data be restricted to frequencies less than 0.05 of the natural frequency of the apparatus. Only at those frequencies can the recorded values be considered to be representative of the actual applied force without the necessity to deconvolve the data from the apparatus response. For our apparatus, this limits recorded forces to frequencies less than ~1 Hz. Such low frequencies were generally not observed during our experiments. To allow the use of higher-frequency data, we also calibrated our force sensor for vertical displacement. A micrometer was used to measure prescribed deflections of the sensor head, which were then correlated directly with the output voltage. This enabled reliable relative displacement measurements, s_z, to be carried out over the required range of frequencies (up to ~100 Hz). These displacement data could be independently verified by comparing their second time derivative, $\ddot{s}_z$, with data recorded by an accelerometer (34103A, ±1g, Summit Instruments) mounted on the flow tube. Although this accelerometer is a three-axis device, only the vertical component (Accz) was used. In Figure 2, the raw and filtered vertical component of accelerometer data are compared with acceleration data derived from the force sensor, for a gas slug ascending through a flare of area ratio 1:4.4. Within the 2–30 Hz band, the accelerations derived from the force sensor accurately match the data from the accelerometer, confirming the reliability of the displacement calibration. Band-pass filtering the data between 2 and 80 Hz also confirms the sensitivity of the force transducer derived accelerations at higher frequencies for which the accelerometer response starts to roll off. Given that the sensors are not located in the same positions (see Figure 1), this could alternatively indicate that higher-frequency oscillations may be absorbed by the plastic (PTFE) seals located between the glass sections up the flow tube, although this is believed to be unlikely. Hence all vertical apparatus accelerations used throughout this paper are derived from the force sensor data. Filtering has been carried out digitally using six-pole Butterworth filters.

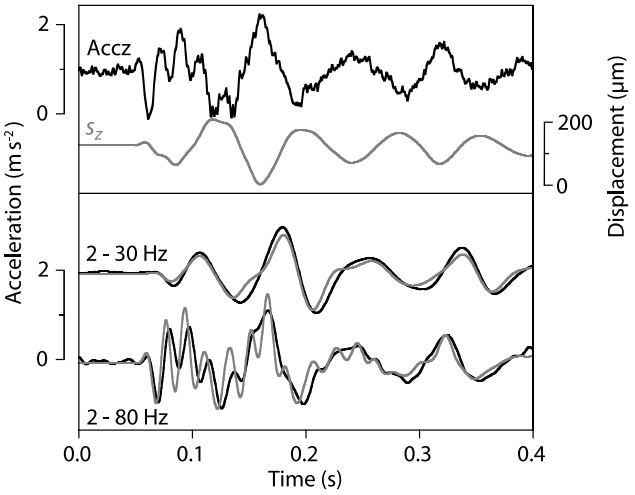

Figure 2. Apparatus acceleration and displacement. The top panel (raw data) shows the vertical component of acceleration recorded by the accelerometer, Accz (black trace), and vertical component of displacement, s_z, obtained from calibration of the force sensor for displacement (gray trace). In the lower panel, band-passed vertical accelerations are shown. The black traces are derived from the accelerometer (Accz) data, and the gray traces have been calculated by twice differentiating the displacement data, $\ddot{s}_z$.

[12] Output voltages from the transducers are sampled at 5 kHz with 16-bit resolution using a National Instruments DAQ board in a PC. The experiments were also recorded visually with a digital video camera (Canon DM-XL1 in FRAME mode) synchronized to the pressure data by including an LED binary counter (incremented by the scan clock of the logging board) within the field of view. Using a shutter speed of 1/1000 s, the digital images can be correlated to the sensor data with an accuracy of ±5 data points (1 ms).

[13] Experiments were carried out using three different pipe sizes with internal diameters of 38, 50 and 80 mm, allowing investigation of three different geometry change ratios (Figure 1b). Here, we consider slug ascent through a diameter increase (a "widening" or "flare"), a diameter decrease (a "narrowing"), and a short section of increased diameter pipe (a "bulge"). Three liquid viscosities (0.001, 0.1 and ~30 Pa s, as measured with falling ball apparatus) were employed by using water, a white cane sugar solution,

and a diluted commercial sugar solution (Golden Syrup), with densities of 1000, 1250 and 1340 kg m^{-3}, respectively.

[14] The volume, V, of gas in a slug is measured by recording the depth of the liquid surface below the release valve. To enable the comparison of results from experiments with different size tubes and slugs, we consider an equivalent aspect ratio, L', for slug size. Assuming a static cylindrical gas volume, with diameter equal to that of the confining tube, L' represents the ratio of the vertical length, L, of the gas volume, to the tube diameter, D:

$$L' = \frac{L}{D} = \frac{4V}{\pi D^3}. \quad (5)$$

Although L and L' are convenient for comparing slug lengths, the shape of the slug nose and the volume occupied by the surrounding falling liquid film are not accounted for; hence accurate slug lengths are not represented directly. In our experiments, the head of liquid above the slug source is always less than 2 m, and the corresponding slug volume increase (<20%) due to reduced static pressure during ascent is deemed to be a secondary effect and is neglected. The repeatability of the processes (evidenced in the geometrical similarity and stability of the slugs prior to their entry in the diameter change region of the flow tube) is illustrated by experiments carried out with identical parameters. Pressure data recorded over ten repeated runs (Figure 3) demonstrate the equivalence of the initial pressure transients generated, even when a severe geometry change induces rapid disruption of the gas slug. Usually, experiments were repeated with identical parameters only five times.

3. Results and Interpretation

3.1. Tube Narrowing

[15] The flow processes that occur during the ascent of a gas slug through a reduction in tube diameter are the least complicated of those observed in our experiments, with steady slug flow established both below and above the tube discontinuity (i.e., with no significant change in flow pattern). Sketches of a typical transition, taken from video frames, are shown in Figure 4a, indicating that as a slug nose impinges upon a diameter reduction, a smaller-diameter slug begins to form. Given that the ascent rate of gas slugs is reduced in narrower tubes ($U_o \approx 0.35\sqrt{(gD)}$ under inertial control), the upward velocity of the slug base strongly decreases as the smaller-diameter segment of slug begins its ascent in the upper, narrower tube. Volume conservation dictates that the smaller-diameter slug is longer than the initial slug, so that L' increases.

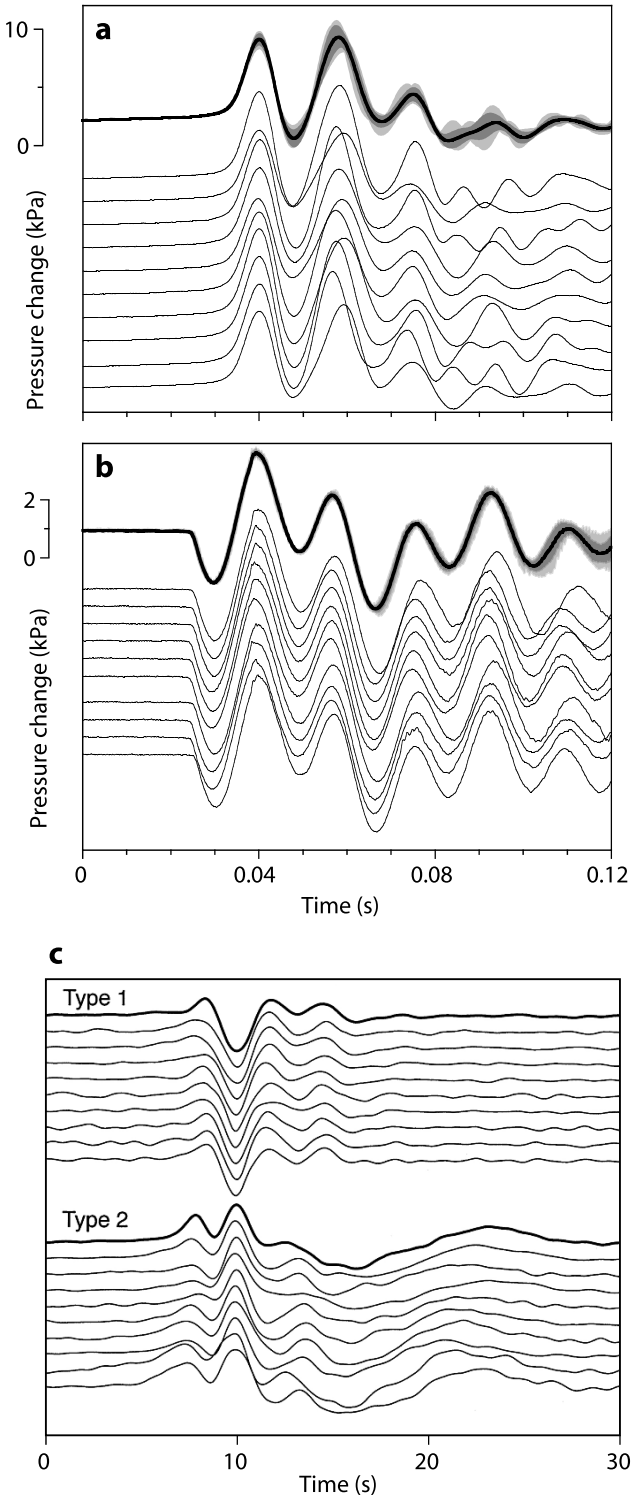

Figure 3. (a) Base (ASG 1) and (b) flare (Pz 5, see Figure 1) pressure data recorded during 10 identical experiments using a gas slug (L' = 4.4) ascending in water (0.001 Pa s) and transiting through a flare with 1:4.4 area change ratio. Data from each experiment have been vertically offset for clarity, and their similarity demonstrates the repeatability of the nondestructive processes involved. The bold black line at the top of each plot represents an average of all the traces below (thin lines), and the dark and light gray patterns superimposed on that line represent the standard deviation and range in signal amplitude, respectively. (c) For comparison, seismic motions of VLP events recorded at Stromboli are reproduced from *Chouet et al.* [2003, Figure 4] in order to demonstrate their similar level of repeatability. Data shown are normalized east components of velocity seismograms for 10 examples of two different types of VLP event. Type 1 events were filtered at 2–20 s, and type 2 events were filtered 2–30 s.

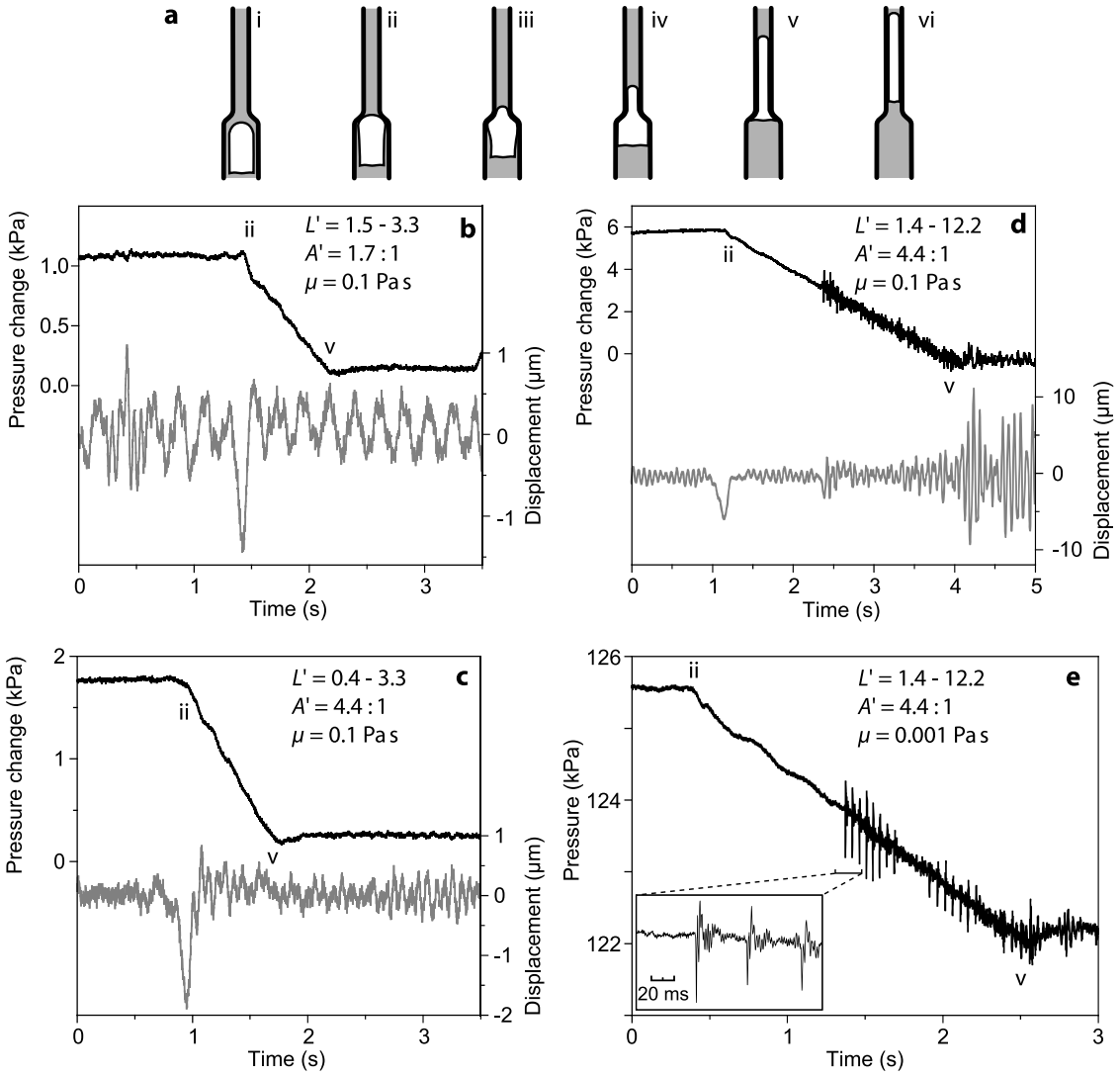

Figure 4. Slug ascent from large to small diameter tube. (a) Sketches of the flow processes observed as a gas slug enters a smaller-diameter tube, and (b–e) the pressure variations and apparatus displacements recorded, with slug position from Figure 4a indicated. Data plotted are ASG 1 pressure (black traces) and s_z displacement measurements (gray traces) from experiments carried out with the values of cross-sectional area change ratio (A'), equivalent slug aspect ratio (L', see equation (5)), and liquid viscosity (μ) indicated in each plot. In Figures 4d and 4e, high-frequency pressure fluctuations believed to be caused by instabilities in the falling liquid film around a long gas slug are seen superimposed on the pressure ramp. The inset in Figure 4e shows details of the series of pressure spikes revealed by the Pz 1 data.

[16] The pressure changes recorded during the passage of gas slugs through reductions in tube diameter (Figures 4b–4e) are dominated by both static and quasi-steady dynamic (i.e., effectively unchanging dynamic) effects [*James et al.*, 2004], rather than dynamic transients (i.e., rapidly changing dynamic effects). The quasi-linear decrease in the ASG 1 pressure data displayed in Figures 4b–4e represents changes in static head and pressure loss around the ascending slug as it passes through the region of tube narrowing (Figure 4a, sketches iii–v). Video data show that the onset of the decreasing pressure ramp coincides with the slug nose entering the narrow tube, and that the ramp end corresponds to the slug tail entering the narrow tube. An estimate of the overall pressure drop can be obtained by using the static gas-volume approach employed in equation (5), where a slug is represented as a stationary gas pocket with the same diameter as the tube. Accordingly, the base pressure change, ΔP_b, resulting from the varying aspect ratio of a slug in different diameter tubes can be expressed as

$$\Delta P_b \approx \rho g L_l' D_l (1 - A'), \tag{6}$$

where L_l' is the equivalent aspect ratio of the slug in the lower tube, D_l is the diameter of the lower tube and A' is the cross sectional area ratio of the flare (cross sectional area of lower tube/cross sectional area of upper tube). This yields an estimated pressure change of −3.8 kPa for the data shown in Figure 4e, in reasonable agreement with the measured pressure drop of 3.4 kPa.

[17] Although the accelerations produced are below the detection threshold of the accelerometer, small transient displacements of the apparatus ($\sim$1–5 μm) are detected as the slug nose enters the region of diameter change (gray traces, Figures 4b–4d). This sharp downward motion is similar in form and magnitude to that produced when a gas slug arrives at the liquid surface in a constant diameter tube. In this "slug at surface" situation, the apparatus motion is driven by a downward-traveling pressure pulse which is attributed to the collapse of the liquid flow field around the slug nose [*James et al.*, 2004]. We consider that changes in the liquid flow field at the slug nose are similarly responsible for the downward motion of the apparatus when diameter reductions are encountered by ascending slugs. However, in this case, an accompanying pressure pulse would be difficult to distinguish over the onset of the larger pressure changes resulting from varying static and quasi-steady dynamic processes. Furthermore, as the slug changes shape upon entering the smaller-diameter tube, pressure changes will be coupling to the apparatus at the diameter change as well as at the base of the tube.

[18] When large diameter change ratios lead to very long slugs in the narrower tube, the length of the falling film of liquid around the slug induces the development of observable flow instabilities within the film. Below the slug, the onset of instabilities is observed as the emergence of high-frequency pressure variations above noise levels. For the 0.1 Pa s liquid in Figure 4d, the onset of high-frequency pressure fluctuations occurs at roughly 2.3 s into the displayed data. In a 0.001 Pa s liquid (water) these instabilities are associated with characteristic, repetitive signals (see events starting 1.3 s into the record of Figure 4e). The frequencies produced range from the repeat period of the signal (about 20–30 Hz, but irregularly spaced) to approximately 600 Hz (inset of Figure 4e). These pulses are believed to correspond to solitary waves [*Lin and Gollub*, 1994] developing in the falling film around long slugs; however, as they are not the primary concern of this paper, a more detailed study is left for further work.

3.2. Tube Widening

[19] Video images show that the transit of a gas slug through an increase in tube diameter can be a considerably more complex process involving changes in flow pattern (Figure 5a). In general, slug ascent velocities are greater in larger-diameter tubes. Therefore when the slug nose enters a larger tube, the downward-flowing liquid flux around the slug nose increases. As this increased liquid flux descends into the smaller diameter tube, the falling liquid film around the slug body thickens and, upon reaching the base of the slug, accelerates the slug base upward into the flare. Relatively small increases in tube diameter (e.g., in our experiments, from 38 to 50 mm) induce only slight flow changes within the falling film and these are accommodated with few observable effects. Greater changes in diameter result in an increased thickening of the falling liquid film in the smaller tube and increasingly rapid ascent of the slug base.

[20] For sufficiently severe increases in tube diameter, the slug nose travels only a small distance through the flare aperture before becoming "detached" from the wall (Figure 5a, sketch iii). The change in the liquid flow field around the slug nose (which determines the slug shape) allows the slug nose to expand sideways. A bulbous head forms as a result, and liquid begins to drain rapidly into the top of the smaller tube, forming a thickening annulus in the falling liquid film (Figure 5a, sketch iv). Consequently, as liquid continues to flow into the falling annulus, an increasingly narrow neck is formed within the slug, just below the base of the flare. Subsequent events then depend on whether or not the annulus grows sufficiently to close the narrowing slug neck before reaching the base of the slug. If the slug neck becomes closed, the downward liquid flux (originally representing the annulus) now forms a liquid "piston" (Figure 5a, sketch v), which temporarily halts the upward gas flow, and disrupts the slug into separate portions. The occurrence of this process is determined by the cross-sectional area ratio of the flare, the liquid viscosity and the slug length (or aspect ratio).

3.2.1. Observations of Inertially Dominated Flows

[21] In the inertially dominated experiments (liquid viscosities of 0.001 and 0.1 Pa s), with flare cross sectional area ratios of 1:4.4, the falling liquid annulus did not close before reaching the slug base for observed slugs shorter than $L' = 3.3$. When this increase in downward liquid flux reaches the slug base, the annulus closes rapidly, producing a single, relatively equant but highly unstable bubble, located just above the flare. This bubble then rapidly elongates by accelerating a narrow, pointed bubble nose upward, reaching velocities of $\sim$1 m s^{-1} (Figure 5b). The bubble nose then decelerates to the steady state velocity of 0.3 m s^{-1} with pressure fluctuations accompanying changes in shape and bubble coalescence at the slug base. Stable bubble shape is regained within the confines of the apparatus, at which point, pressure fluctuations subside.

[22] The majority of the slugs used in our experiments were sufficiently long ($L' \geq 3.3$, Figures 5a and 5c) that the whole slug body could not enter the larger diameter tube before the narrowing neck was closed by the growing liquid annulus. As a result, successive sealing of falling annuli formed a series of short, liquid "pistons" that sequentially disrupted ascending slugs into several separated sections. On the first occurrence of this process, the detached bubble in the flare accelerates upward in the jet-like manner (Figure 5a, sketch vi; Figures 5c and 6) described above, with nose velocities of up to 2.8 m s^{-1} being noted (averaged over 0.04 s). Maximum nose velocities occurred in experiments carried out with $L' = 3.3$, the smallest slugs for which breakup was observed. These velocities are nearly an order of magnitude larger than the maximum steady ascent velocity of 0.3 m s^{-1} for inertially controlled slugs (in a 0.08-m-diameter tube). The exact process responsible for the jet-like ascent of the bubble is not known but we hypothesize it must be the result of transient pressure gradients generated by the arrival of the bubble and its unstable, "equant" shape in the base of the larger tube. Fluctuations in the diameter of the jet bubble nose are visible as longitudinal waves propagating down the sides of the bubble (Figure 6).

[23] After ascending a distance of 0.3–0.4 m (covered in a time of 0.16 s spanning four video frames), the bubble nose stalls, the base catches up, and the bubble becomes disrupted into a series of smaller bubbles by flow instabilities and wake turbulence. These bubbles are considerably

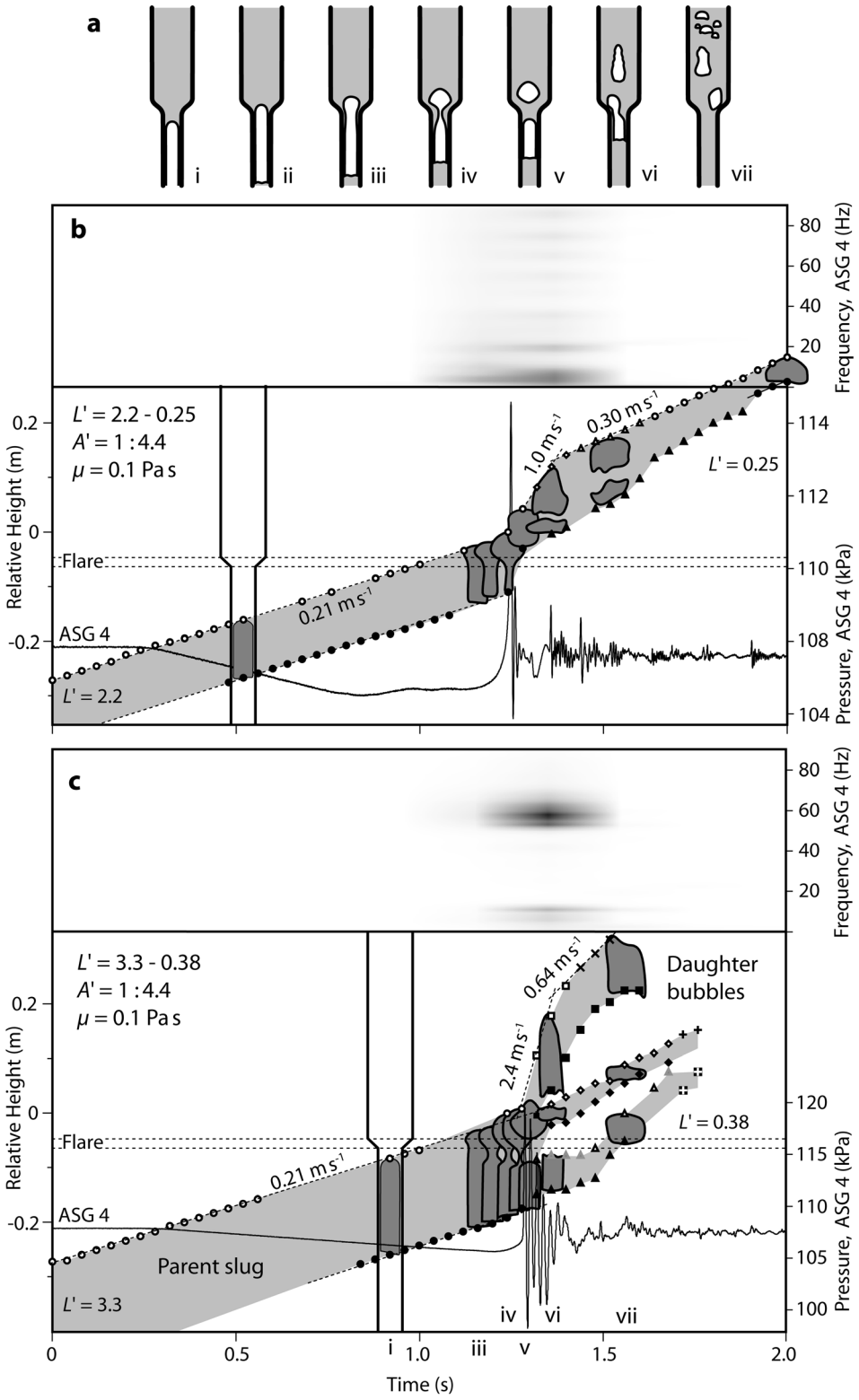

Figure 5. Slug ascent from small to large diameter tube. (a) Sketches of flow processes observed as a long parent gas slug ($L' \geq 3.3$) is broken up into daughter bubbles (see text for details). (b, c) ASG 4 pressure data and spectrograms are shown along with slug shapes and space-time fields taken from video frames. Open symbols represent positions of the slug (or bubble) nose recorded in individual video frames, and closed symbols represent the positions of the slug base. In Figure 5b, a small slug ascends into the larger tube without being broken up in the flare. The slug is disrupted by turbulence shortly after entering the larger tube, with the daughter bubbles rapidly coalescing. We distinguish this from breakup within the flare, which is illustrated for a larger slug in Figure 5c.

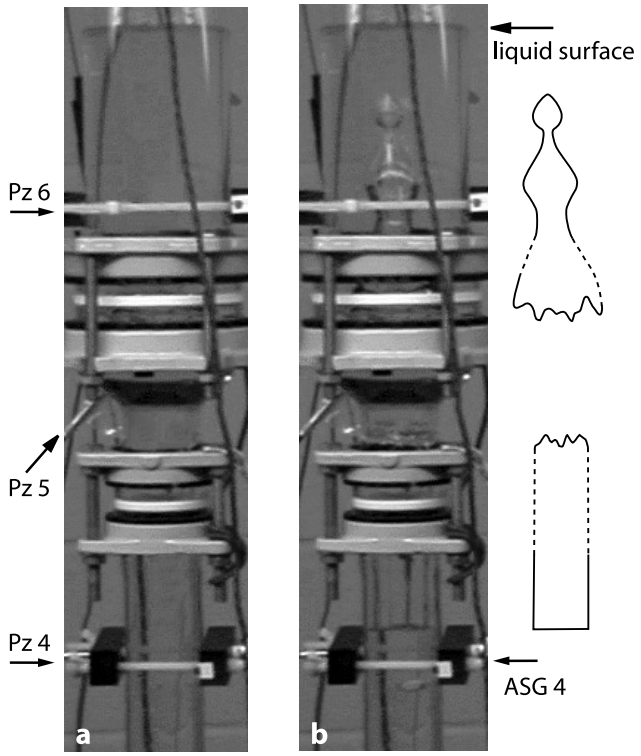

Figure 6. Still images taken from digital video (a) without and (b) with the bubble nose ascending in a jet-like manner immediately after slug disruption in the flare. Liquid viscosity is 0.1 Pa s, cross-sectional area change ratio, 1:4.4, and the initial slug aspect ratio is 4.4. To the right of the images, a sketch of the slug outline in Figure 6b is given. Note the unstable and dynamically controlled shape of the bubble nose as well as its irregular base, indicative of turbulence. The lower section of the original slug, still in the smaller tube, also has an irregular but flat (rather than domed) upper surface but retains its steady state base.

smaller than the maximum stable bubble size for stagnant media [*Clift et al.*, 1978, Table 12.3], pointing to the unstable and transient nature of the processes involved. During this period, the segment of slug remaining in the lower tube continues to rise until the process of neck formation repeats itself. However, in low-viscosity liquids, the symmetry displayed in the first slug nose through the flare is subsequently considerably reduced by the turbulence induced by the initial event.

3.2.2. Observations of Viscosity-Controlled Flows

[24] In more viscous liquids (~30 Pa s in our experiments), where slug ascent is controlled by viscosity, slug disruption can be observed in "slow motion," with disruption occurring for observed slugs with $L' \geq 2.2$. Initially, a near-spherical daughter bubble is generated from the original slug nose (bubble 2, Figure 7a). This is shortly followed by the growth of a second near-spherical daughter bubble, almost identical in size and ascent velocity. Suppression of turbulence by the high liquid viscosity during the slug breakup process allows the production of these self-similar daughter bubbles, which are close to their maximum stable size [*Clift et al.*, 1978, Table 12.3] and maintain their relatively spherical shape until they reach the liquid surface. The rapid, jet-like ascent of bubble noses after separation from the slug body is not observed under viscous control.

[25] Longer parent slugs are broken up into larger numbers of near-spherical daughter bubbles. For $L' = 6.6$, the breakup process generated nineteen daughter bubbles from the original parent slug, of which eight reached the surface in three discrete groups (of three, four, and one bubble), as shown in Figure 7b. The first two bubbles in the first two groups (space-time fields 2, 6 and 8, 10 in Figure 7b) were nearly identical in size and ascent velocity. This initial "double bubble" separation process was not observed when significant inertial influences (and turbulence) were present. Subsequent bubbles were less regular in size (space-time fields 7, 12 in Figure 7b), allowing, due to differences in ascent velocity, bubble collisions and coalescence (space-time fields 12, 14 and 18, 19 in Figure 7b) to take place.

3.2.3. Pressure and Displacement

[26] In contrast to the processes associated with slugs ascending through diameter reductions, significant transient pressure changes are frequently produced when slugs ascend through increases in tube diameter. In our experiments, the largest pressure changes were recorded by ASG 4 and Pz 4 (located just below the flare, Figure 1a) under inertially controlled conditions. Figure 5b illustrates the typical processes observed for slugs that were too short to undergo disruption in the flare. Notice the coincidence of a short pressure pulse (~10 kPa) with the closing of the falling liquid annulus, and the formation of an equant bubble above the flare. Smaller signals (<4 kPa) are associated with the processes of bubble breakup, coalescence and oscillation as the equant bubble regains an equilibrium shape at about 1.9 s. Figure 5c illustrates the slug disruption in slugs that did break up during transit through the flare. The slug breakup is accompanied by stronger pressure oscillations (~20 kPa) that are induced by the closure of the gas neck, forming a "liquid piston."

[27] Unfortunately, the presence of the lower portion of the gas slug traversing the ASG/Pz 4 region at the same time complicates the interpretation of these data. Therefore to facilitate visual comparisons between experiments carried out with different geometries and slug sizes, we first focus our attention on the data recorded by the ASG 1 and Fz transducers (Figure 8) located at the base of the apparatus (Figure 1a). Common to all plots in Figure 8 is an overall pressure increase resulting from the changing static pressure (equation (6)) and steady dynamic pressure losses associated with gas slug ascent in the different diameter tubes. Superimposed on these offsets are oscillatory pressure disturbances with amplitudes ranging from ~0.5 kPa for a small slug and small widening (Figure 8a) up to ~5 kPa for a large slug and large widening (Figure 8f). As demonstrated in Figure 3, the onsets of the pressure waveforms show a high degree of reproducibility between "identical" experiments. However, in the case of long slugs where multiple slug breakup events result in extensive turbulent wakes (Figures 5a and 8f), only average pressure magnitudes are repeatable at longer timescales.

[28] Although it is difficult to correlate the morphology of the pressure signals among the different plots in Figure 8, common features can be identified and traced between experiments when a more extensive experimental suite is considered. As an example, Figure 9 displays results

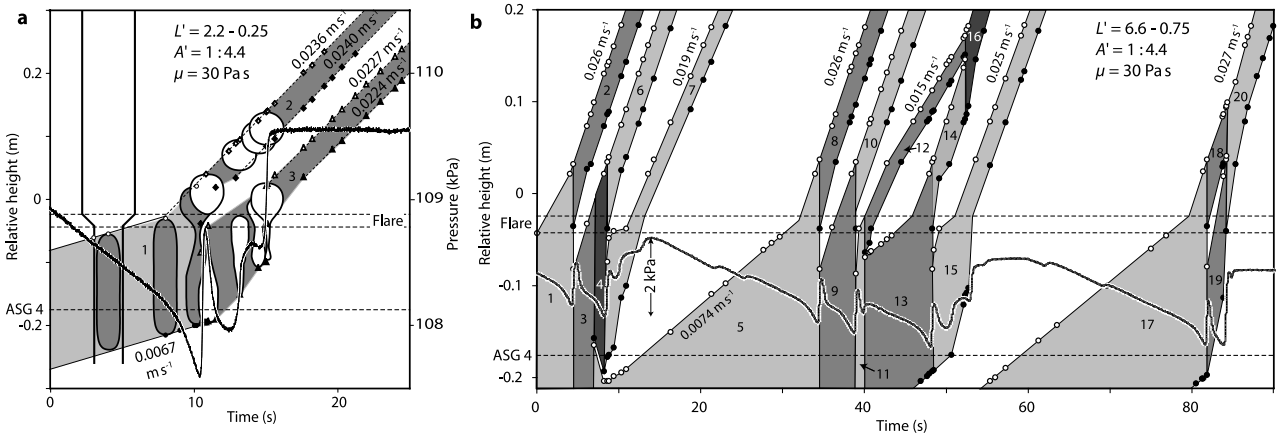

Figure 7. The flow behavior of viscous controlled slugs ascending through a flare. (a) Slugs just sufficiently large (space-time field labeled 1) to break up within a flare generate two daughter bubbles (space-time fields 2 and 3). Slug shapes sketched from selected video frames are shown. (b) Longer gas slugs break up and generate many daughter bubbles, some of which coalesce before reaching the surface. The space-time fields are labeled 1 for the parent slug and 2–20 for the daughter bubbles. Some of the breakup events leave a new slug nose to form at a considerable distance below the flare, e.g., daughters 5 and 17, which themselves become the parents for the next bubble train. Data points represent slug observations from individual video frames, with open symbols representing the bubble/slug nose and closed symbols the tail. ASG 4 pressure data are shown by the irregular black trace, with the sensor position given by the labeled dashed line.

obtained over a more complete range of slug aspect ratios including values intermediate between those illustrated in Figures 8a and 8d (for a cross sectional area ratio 1:1.7). The rapid pressure change at the start of the static ramp at ~1.7 s in Figure 8a for a "small" slug is related to the onset of the pressure spike at ~1.3 s in Figure 8d for a "large" slug. The small "overshoot" transient at the top of the ramp (at ~2.0 s in Figure 8a) corresponds to the more gradual pressure "overshoot" at ~2.2 s in Figure 8d. Features associated with the onset of the static pressure ramp (indicating the decreasing aspect ratio of the slug as it expands sideways in the flare) and the return to a constant DC pressure (indicating the gas is entirely in the large tube, or has escaped from the liquid surface), can be observed in all panels in Figure 8. Thus the overall morphology of the pressure changes can be correlated directly with physical parameters such as slug size and magnitude of the discontinuity.

[29] Under viscous control, little oscillatory pressure behavior and no apparatus displacements are recorded (Figure 10, compare to Figure 9b). The slow liquid speeds involved in these experiments simplify the correlation of pressure measurements to physical flow processes (Figure 7a). Figure 10a shows the pressure recorded by ASG 1 as a slug ascends from a small- into a medium-diameter tube (cross sectional area ratio 1:1.7) without being broken up. The overall pressure increase (~1.5 kPa) due to the change in static and steady dynamic effects is similar to that observed for the same tube geometry and slug size in low-viscosity liquids (~1.3 kPa, Figure 9b). No pressure change is detected as the slug nose enters the widening at ~0.7 s. The onset of decreasing pressure at 1.1 s coincides with an observed increase in the downward-directed liquid flux, marked by a thickening of the liquid film falling around the body of the slug. We interpret this pressure decrease as due to the increased volume (mass) of liquid being viscously supported by the tube walls during this film thickening and, therefore, not contributing to measured pressure at the base of the liquid column. This is consistent with any displacement of the apparatus being undetectable; the reduced downward force on the tube resulting from the decreased liquid pressure at its base is fully balanced by the added weight of the viscously supported liquid mass on the tube walls. When the increased flux in the falling film reaches the level of the slug base, the slug base accelerates upward and a steep pressure increase is recorded (interval 1.3–1.4 s in Figure 10a), reflecting the wall-supported mass rejoining the liquid column as well as slug geometry changes. A small-amplitude pressure pulse is measured immediately after this process, and is interpreted to be the result of a heavily damped oscillation as the bubble regains an equilibrium shape.

[30] Figure 7a illustrates the sequence of bubble motions, together with ASG 4 pressure data, for a slug with initial $L' = 2.2$ transiting through a flare with area ratio 1:4.4. In this case, the widening is sufficient to induce a disruption of the slug into two daughter bubbles. Figure 10b displays the pressure response obtained when a larger slug with initial $L' = 4.4$ ascends from a small- into a large-diameter tube in a high-viscosity liquid (compare with Figures 7a, 8c, and 8f under inertially dominated conditions) yielding four daughter bubbles in two trains. Initially, the pressure trace is similar to that seen in Figure 10a, displaying a small pressure decrease resulting from wall support of the thickening liquid film after the slug nose entered the larger diameter tube. The onset of the first pressure increase corresponds to the apparent closing of the narrowing gas neck (see Figure 7a), which forms a detached bubble from

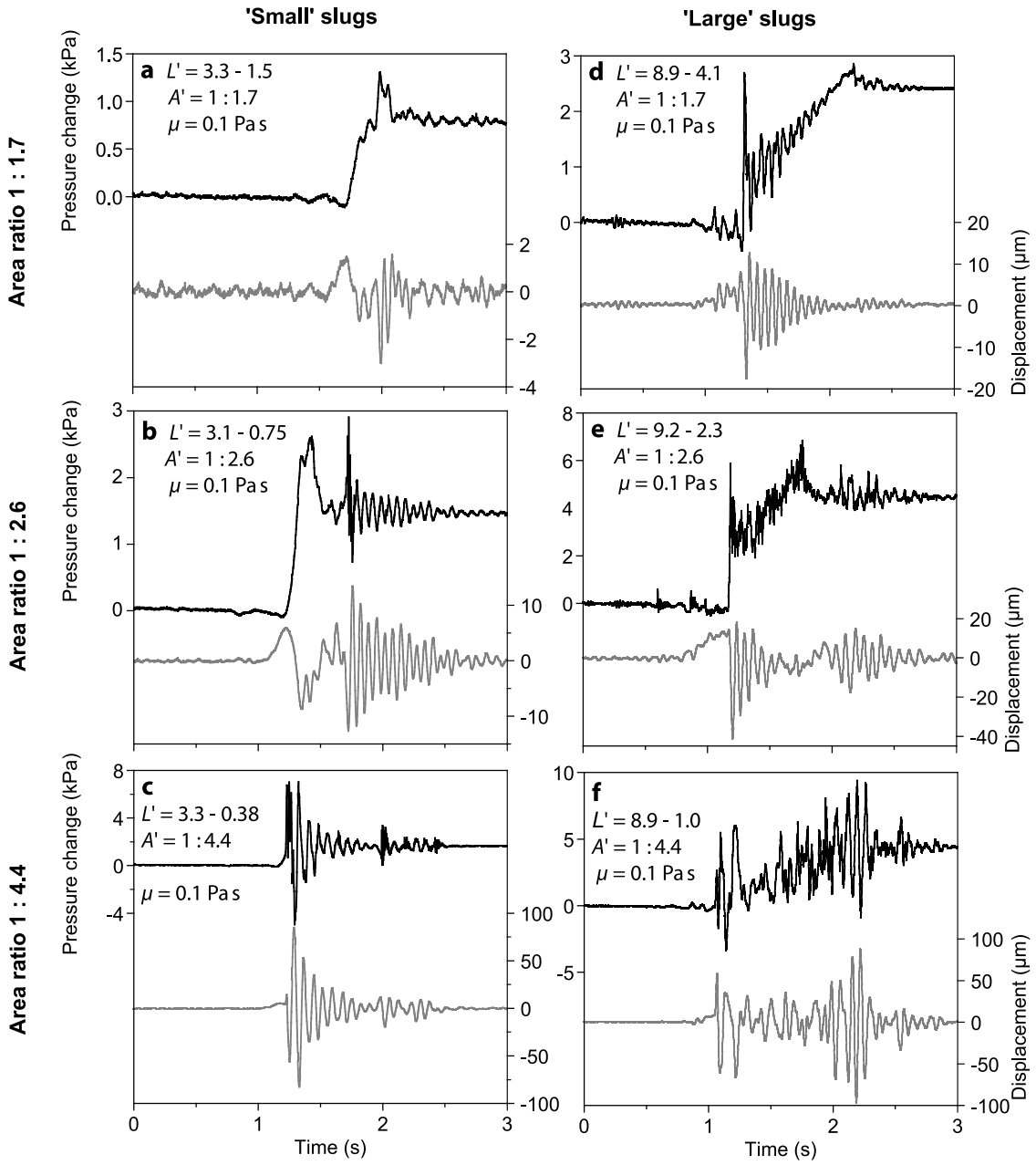

Figure 8. Pressure measured by ASG 1 (black traces) and apparatus displacement, s_z (gray traces), during the ascent of "small" (left-hand plots) or "large" (right-hand plots) slugs in tubes with different cross-sectional area change ratios, A' (see Figure 1b). A', the equivalent slug aspect ratio (L', see equation (5)) for each slug (in the small and then the large tube), and the liquid viscosity, μ, are indicated in the upper left corner of each panel. With the exception of Figures 8c and 8f, the pressure increases displayed are dominantly due to the changes in static and dynamic pressures associated with the slug rising in a tube of increased cross-sectional area (equation (6)). However, even in these cases, significant oscillation of the apparatus was observed in the s_z data. In Figures 8c and 8f the dominant pressure changes are oscillations induced by the disruption of the slug within the flare. Figure 8c is the same experiment as that seen in Figure 5c, where the ASG 4 pressure response and slug space-time field is shown.

the original slug nose. However, pressure immediately starts to decrease again as a second bubble begins to form directly behind the first separated bubble, in the region originally part of the first bubble neck. Only when this second bubble has detached from the remainder of the slug does pressure increase again (at 14 s in Figure 10b) due to slug geometry change. The small pressure steps at 20 and 27 s are due to these two initial bubbles bursting at the surface of the liquid. This symmetric double bubble detachment is repeated again at ~40 s (Figure 10b) as the remainder of the slug passes through the flare. These same features can be identified in the flow behavior of longer slugs (Figure 7b), where double

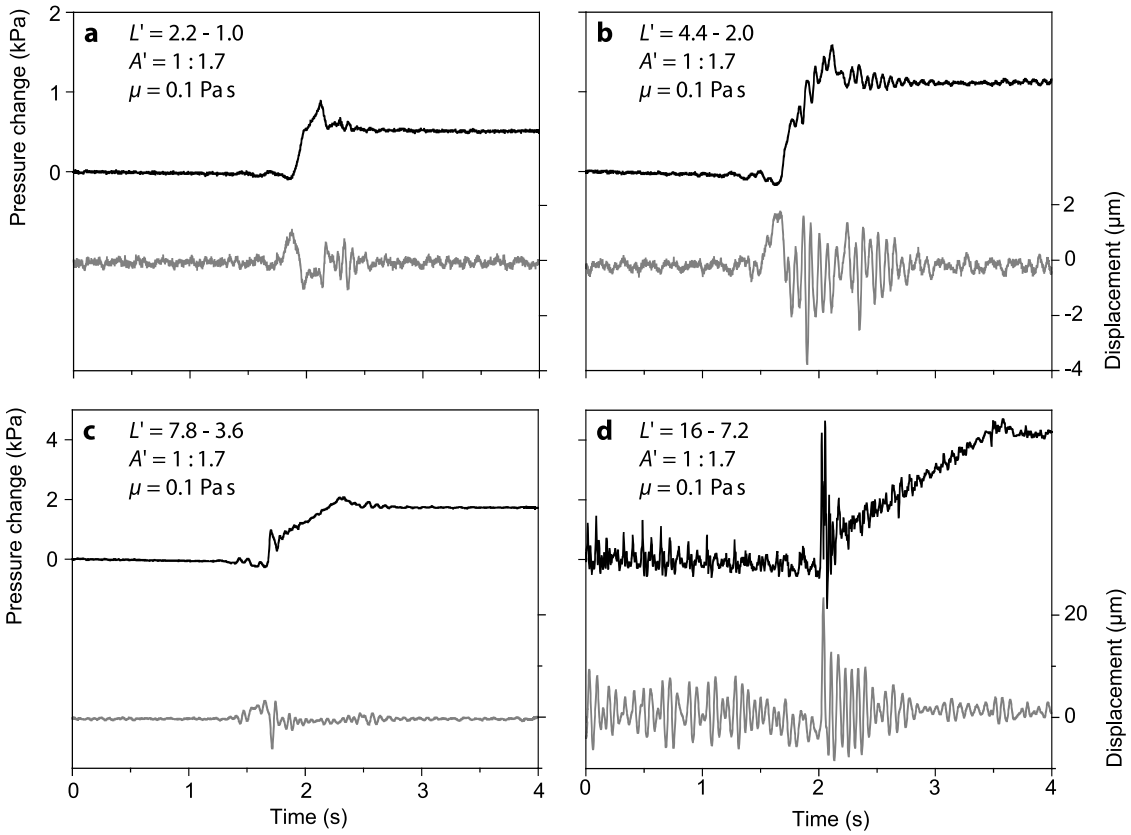

Figure 9. Variation of pressure recorded by ASG 1 (black traces) and apparatus displacement, s_z (gray traces), during the ascent of gas slugs of different sizes in a tube with fixed cross-sectional area increase ratio 1:1.7. These results demonstrate how the seemingly different pressure waveform shapes in Figures 8a and 8d are related, with the slug length increasing in the order of Figures 9a, 8a, 9b, 9c, 8d, and 9d. Note the elevated background levels of resonant apparatus oscillation stimulated by the turbulent wake in the longest slug (Figure 9d).

bubble detachment appears to precede the generation of more complex bubble groups within the bubble train created as the slug traverses the flare.

3.2.4. Oscillatory Sources

[31] As demonstrated in Figure 8, the largest pressure changes occur during slug breakup induced by a tube widening with cross-sectional area ratio of 1:4.4 in low-viscosity liquids (e.g., Figures 8c and 8f). Large pressure transients always occur at the beginning of the static pressure ramp, although significant signals are also observed at the end of the ramp for long slugs (Figure 8f). Examples of ASG 1, ASG 4, and s_z data (derived from Fz) recorded with this tube geometry and an L of 4.4, changing to 0.5 in the larger tube (similar to Figures 5c and 8c), are given in Figure 11a. The downward ramp in the ASG 4 data (also seen in Figures 5b and 5c) marks the interval during which the body of the gas slug is passing by this transducer [*James et al.*, 2004], which is located just below the flare (Figure 1). Little change is recorded by this transducer as the slug nose enters the flare (at 1.0 s). Within the temporal resolution of the digital video (0.04 s), the sharp onset of the pressure transient observed at ~1.3 s coincides with the top portion of the slug becoming detached from the remainder of the ascending slug due to closure of the gas neck after passage of the slug nose through the widening (between sketches iv and v in Figure 11a). The frequency content of subsequent pressure oscillations at Pz 4 and Pz 1 is illustrated in Figures 11b and 11c, respectively. The spectrograms show three different frequency components: (1) a "high"-frequency component at ~60 Hz; (2) a "low"-frequency component at ~6 Hz; and (3) an "intermediate"-frequency component at ~13 Hz, apparent mostly at Pz 1. Pz 1 also shows evidence of broadband signal in the initial transient.

[32] Considering the ~13 Hz oscillations first (which persist throughout the Pz 1 data, Figure 11c), we note that this is the natural resonant frequency of the entire spring-suspended apparatus resting on the force transducer. This component is, therefore, likely to reflect pressures induced in the fluid by vertical resonant oscillation of the surrounding apparatus on its springs. This is verified by examination of the phase relationship between the pressure recorded at the base of the apparatus (Pz 1) and the apparatus acceleration. Figure 11d shows that both pressure and acceleration data display persistent, in-phase 13 Hz oscillations with slowly decaying amplitudes. This phase correspondence confirms that apparatus motion is responsible for inducing the observed liquid pressures, whereby an upward acceleration of the apparatus increases the liquid pressure at the base of the tube, which in turn accelerates the liquid

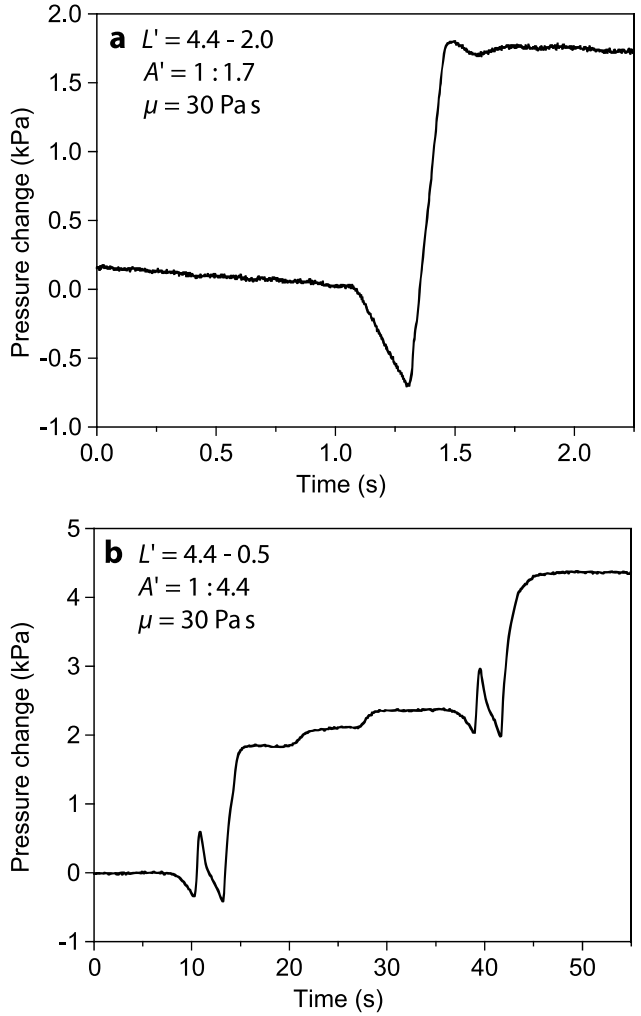

Figure 10. Pressure changes recorded by ASG 1 during the ascent of gas slugs through a flare under viscous control. (a) A relatively short gas slug rises through a small diameter increase without breaking up. Onset of the sharp pressure decrease (1.1–1.3 s) corresponds to observed increases in the downward liquid flow rate into the top of the smaller tube as the slug nose enters the wider-diameter tube. The reduced pressure is therefore interpreted to reflect the increase in the amount of liquid being viscously supported on the walls of the flow tube. When the increased liquid flow reaches the base of the slug, pressure rapidly increases, and the slug base accelerates upward into the upper tube. (b) Data for a gas slug ascending through a severe diameter increase (compare with Figure 7). In this case the slug is broken up in the transition to the larger-diameter tube, forming two daughter bubbles above the flare during the interval 10–14 s (which reach the surface at 21 and 27 s) and repeating the process near ~40 s.

column upward ("following" the apparatus). Further support for this mechanism is found in the greatly reduced amplitude of the 13 Hz component at Pz 4 (see spectrogram in Figure 11b), reflecting the reduced head of fluid above this transducer [*James et al.*, 2004]. Accordingly, in-phase pressure and acceleration data are the result of the apparatus's mechanical response to an initial vertical perturbation and, as such, this 13 Hz frequency component is specific to our apparatus and we do not consider it to be part of a "source" process.

[33] In contrast, the high-frequency components of the pressure and acceleration data present during the first ~0.1 s (approximately six cycles) of the oscillatory transients demonstrate a clear out-of-phase relationship (inset of Figure 11d). This out-of-phase correlation is consistent with an acceleration of the apparatus being driven by changes in liquid pressure (i.e., elevated fluid pressure acting on the base of the tube accelerates the apparatus downward). The high-frequency, ~60 Hz component thus represents a fluid-driven process distinct from the resonant mechanical response of the apparatus. Details of the high-frequency onsets of the pressure transients recorded at different levels in the tube are shown in Figure 11e. The onset of the sharpest pressure change occurs during the time interval between the last video frame in which the body of the slug is still joined to the bulbous nose entering the flare by a narrowing neck (sketch iv), and the following frame, in which the closing of the gas neck has separated the slug into two bodies (sketch v). Transducers Pz 4 and Pz 5 (see Figure 1 for position) detect pressure changes almost simultaneously (Figure 11e), suggesting that the source event occurred somewhere between these two transducers. Pressure sharply decreases at Pz 5, and sharply increases at Pz 4. The decreased pressure in and above the tube widening (Pz 5 and Pz 6) reduces the vertical component of force exerted by the liquid on the flare shoulder. As a result, the apparatus begins to accelerate upward as indicated by the $\ddot{s}_z$ trace at 1.29 s in Figure 11e.

[34] Above the flare, Pz 6 detects pressure change virtually simultaneously with Pz 5. With bubble-free water between Pz 5 and Pz 6, a pressure wave propagation time of ~0.4 ms is expected for a sound speed of ~1500 m s^{-1} in water. This equates to two data points and represents the detection limit for the logging rate used. Below the flare, the onset of pressure increase at Pz 3 occurs ~3 ms after the onset of pressure increase at Pz 4, consistent with a downward-traveling wave propagating at ~200 m s^{-1}. This is not an unreasonable sound speed (requiring only ~0.4% gas bubbles by volume [*Kieffer*, 1977]) in light of the fact that this region of the fluid includes the base of the slug and bubbles entrained in its wake. The onsets of the pressure waveforms at Pz 2 and Pz 1 are slightly distorted by an upward-traveling pressure wave generated at the apparatus base by the previously induced upward acceleration of the apparatus (note the perceptible increase in pressure rise at 1.29 s at Pz 1). After approximately one period of oscillation, the piezo-transducer data are either in phase (Pz 2, Pz 5, and Pz 6), or out of phase (Pz 3 and Pz 4) with Pz 1, indicative of the excitation of a resonant standing wave field within the fluid column (Figure 11e). This phase relationship is maintained during the following ~0.1 s, pointing to a relatively constant distribution of liquid and gas phases during this time period. After ~0.1 s the correlation becomes difficult to observe, suggesting that changes in the distribution of liquid and gas phases may have become sufficiently significant to suppress the resonance. The complex nature of the standing wave (with pressure nodes located between Pz 2 and Pz 3 and between Pz 4 and Pz 5) likely reflects the heterogeneous composition of the reso-

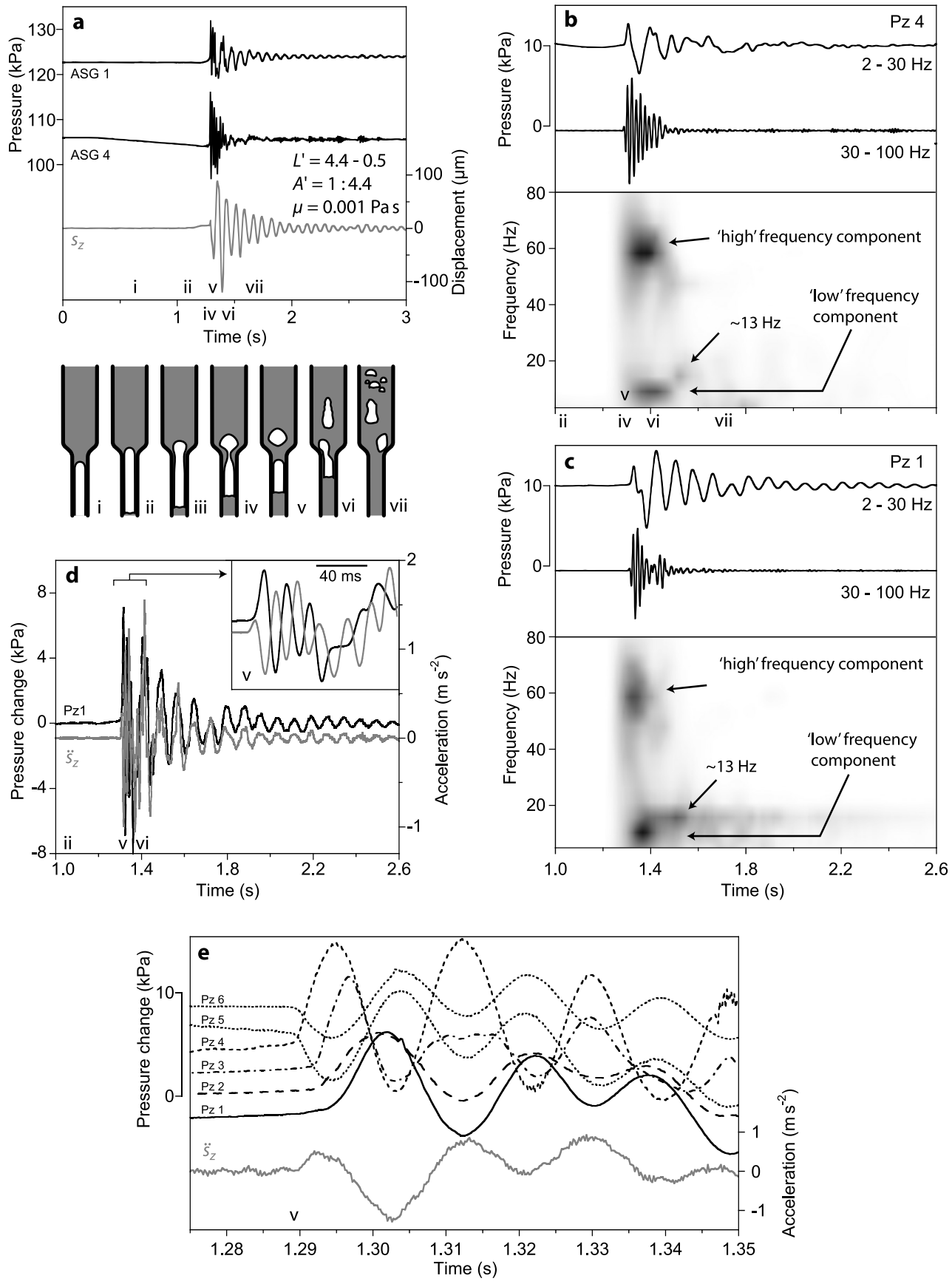
a
Pressure (kPa)
ASG 1
ASG 4
L' = 4.4 - 0.5
A' = 1 : 4.4
μ = 0.001 Pa s
Displacement (μm)
Time (s)
i ii iii iv v vi vii
b
Pz 4
2 - 30 Hz
30 - 100 Hz
Frequency (Hz)
'high' frequency component
'low' frequency component
~13 Hz
c
Pz 1
d
Pressure change (kPa)
Pz1
40 ms
Acceleration (m s-2)
e
Pz 6
Pz 5
Pz 4
Pz 3
Pz 2
Pz 1

Figure 11

nating body resulting from the spatially varying ratios and dispersions of gas within the liquid column. If one assumes the 60 Hz represents a simple organ pipe resonance, then a wave velocity of 200 m s^{-1} (estimated from the initial downward-traveling pressure transient) yields a half wavelength of ~1.7 m. This is consistent with the dimensions of our fluid column. We therefore attribute the short-lived "high"-frequency (~60 Hz) component to an acoustic resonance within the fluid column.

[35] This resonance is excited by a trigger event located between Pz 4 and Pz 5, and occurs within the period of initial slug disruption. Under conditions of no slug disruption in the flare (when a liquid piston was not formed), closure of the liquid annulus at the base of the slug produced a substantial broadband pressure pulse of duration ~20 ms, and peak-to-peak amplitude ~10 kPa (Figure 5b). This pulse duration is close to the period (~17 ms) of the high-frequency resonance observed when the slug is disrupted in the flare (Figure 5c). The trigger mechanism for the high-frequency resonance could, therefore, be the rapid radial deceleration of liquid in the annulus at the point of closure; a process that must take place in both cases. However, differences between the no slug disruption and slug disruption cases such as initially decreasing pressure transients within and above the flare during disruption (Figure 11e), in contrast to initially increasing pressures in the absence of disruption, indicate that there certainly are further complexities involved.

[36] The low-frequency (~6 Hz) component in the spectrograms of Figures 11b and 11c has a duration of <0.2 s, or approximately one period, suggesting that this is either a heavily damped resonance, a resonance with period similar to the timescale of changes in liquid-gas distribution, or is not a resonance at all. In other experiments, this component was observed over two to three periods, suggesting resonance might be playing a role. The short duration and proximity of this frequency to the resonant frequency of the apparatus (~13 Hz) prevent an accurate determination of the phase relationship between pressure and apparatus acceleration and make identification of its origin difficult. However, the similar amplitudes recorded at ASG 1 and ASG 4 (compared to the amplitudes of the 13 Hz signal, in the spectrograms of Figures 11b and 11c) suggest that it is probably not due to the mechanical response of the apparatus, but is a direct result of fluid processes.

[37] Figures 11b and 11c show that the high- and low-frequency components emerge quasi-simultaneously, raising the possibility that they are stimulated by the same physical process, that is the closing of the gas neck and formation of the liquid piston. However, the order of magnitude difference in frequency suggests that the oscillatory processes involved are not likely to be similar. With the high-frequency component attributed to acoustic resonance, a possibility for the low-frequency component might be an inertial oscillation of the liquid. Here, we propose that this depicts the motion of the liquid perched on top of the newly formed gas spring represented by the portion of the slug remaining in the lower tube. When the gas neck closes, momentum in the descending liquid piston must compress the underlying gas, exciting slug oscillation. This hypothesis is discussed further in the following section where the frequencies and amplitudes predicted by such a model are compared with recorded data.

3.2.5. Amplitudes and Frequencies

[38] Figures 8–10 provide an indication of the magnitudes of pressure change that occurred in experiments featuring tube diameter flares. In viscosity-controlled systems (Figures 7 and 10), the lack of significant rates of change of liquid inertia implies that measured pressure changes are reflecting only variations of static head and steady dynamic pressure losses around the slug. When liquid inertia is important (Figures 5, 8, and 9) the amplitudes of pressure transients can exceed these pseudo-static pressure changes and represent a significant fraction of the absolute static pressure. Peak pressure amplitudes measured at the base of the apparatus demonstrate complex variations with parameters such as slug size, believed to result from varying degrees of constructive interference between oscillations generated by different processes.

[39] For small slugs that do not break up ($L' < 3.3$, or $L <$ 12.5 cm in the smallest tube used), the liquid piston never forms, and the fluid processes believed to generate the largest pressure changes (<25 kPa) do not operate, even though, under inertial control, dynamic pressure pulses (<10 kPa, Figure 5b, interpreted to be due to the deceleration of slumping liquid) are larger than the static pressure steps (<2 kPa, Figures 7 and 10, dominantly due to increases in liquid head) produced under viscous control. The largest oscillatory pressure changes were recorded at ASG 4 and Pz 4 (Figures 5 and 11) when slugs ascended

Figure 11. Pressure and displacement transients induced by slug disruption during slug ascent through a severe flare in a low-viscosity fluid. (a) Pressure and displacement data recorded as the gas slug traverses the wider-diameter tube. Flow configuration is indicated with reference to the sketches i–vii. (b) Band-pass-filtered data from Pz 4 (top panel) and spectrogram of Pz 4 data obtained with a 0.2-s-long window moving in 0.01-s increments along data band-passed between 2 and 100 Hz (bottom panel). (c) Same as Figure 11b for Pz 1 data. Both data sets from Pz 4 and Pz 1 show dominant frequency components at ~60 and ~6 Hz. Pz 1 data also indicate an additional long-lived component at ~13 Hz, attributed to oscillation of the apparatus. (d) Comparison of band-pass-filtered (2–100 Hz) Pz 1 data (black trace) and apparatus acceleration (gray trace, calculated from the s_z data). The lower-frequency (~13 Hz) oscillations in the signal coda are in phase, while the initial, higher-frequency (~60 Hz) oscillations are clearly out of phase (see inset). These phase relationships indicate that the 60 Hz signal represents liquid pressures moving the apparatus, whereas the 13 Hz signal is a result of apparatus motion inducing pressure changes in the liquid column (see text for detailed explanation). (e) Details of the initial pressure transients at all the piezo transducers and associated apparatus acceleration calculated from s_z (data are vertically offset for clarity). After the first period of oscillation, in which the progress of a downward-traveling pressure wave can be observed (Pz 4 to Pz 1), data from the piezo transducers appear to maintain constant in-phase or out-of-phase relationships.

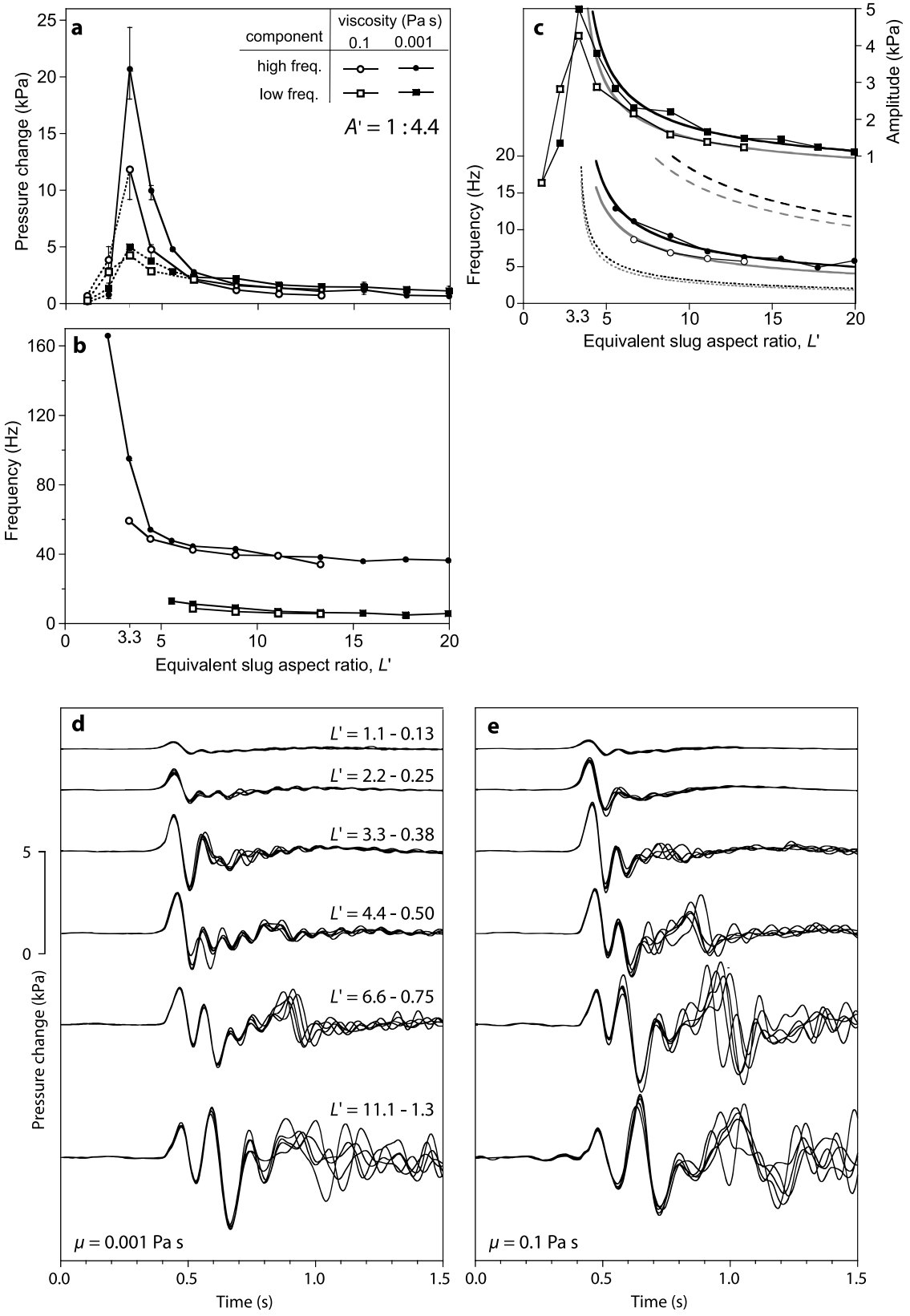
a
Pressure change (kPa)
component
viscosity (Pa s)
0.1
0.001
high freq.
low freq.
A' = 1 : 4.4
b
Frequency (Hz)
Equivalent slug aspect ratio, L'
c
Frequency (Hz)
Amplitude (kPa)
Equivalent slug aspect ratio, L'
d
L' = 1.1 - 0.13
L' = 2.2 - 0.25
L' = 3.3 - 0.38
L' = 4.4 - 0.50
L' = 6.6 - 0.75
L' = 11.1 - 1.3
Pressure change (kPa)
μ = 0.001 Pa s
Time (s)
e
μ = 0.1 Pa s
Time (s)

Figure 12

through a 1:4.4 area-ratio flare in low-viscosity liquids. Figure 12a shows the maximum amplitude of the pressure for the high- and low-frequency components of the initial oscillatory pressure transients as a function of L for the two liquid viscosities 0.1 Pa s and 0.001 Pa s. With sufficient flow distance for the thickening liquid annulus to close, the amplitudes of the resulting pressure oscillations reach a maximum for both viscosities. The 10 kPa pressure pulse apparent in Figure 5b ($L' = 2.2$) as the liquid annulus closes does not appear to contribute to either the high- or low-frequency components in Figure 12a. This is consistent with this pressure pulse being broadband in nature and the absence of suitable physical conditions for it to excite resonance. The peak oscillation amplitude in Figure 12a corresponds to the smallest-sized slug ($L' = 3.3$) that underwent disruption within the flare. Maximum bubble nose velocity (Figure 5c) and apparatus displacement (Figure 8c) also occurred under these conditions. In this case, only a small portion of the original slug remains in the lower, narrower tube after the slug nose has become detached, and a recognizable secondary slug nose never forms (Figure 5c). Pressure changes are larger under full inertial control (viscosity 0.001 Pa s), compared with flows under mixed viscous and inertial control (viscosity 0.1 Pa s). With increasing slug length, maximum initial transient amplitudes appear to approach a near constant value of approximately 1 kPa in both high- and low-frequency components.

[40] Figure 12b shows the dominant frequencies associated with the high- and low-frequency components as a function of L'. The high-frequency component displays a strong frequency decrease with increasing slug size for $3.3 < L' < 7$. This is thought to reflect the increasing amount of gas and entrained bubbles below the flare, which significantly decreases sound speeds (and hence also frequencies) within the fluid column. This interpretation is supported by an observed slowing of the initial downward-traveling pressure pulse with increasing slug size. The absence of high-frequency component at small L' values in the 0.1 Pa s liquid may indicate a viscous damping of the trigger mechanism (the point of closure of the liquid annulus), which otherwise excites the high-frequency signal, or an absence of bubbles in the liquid to slow the sound speed [*Kieffer*, 1977] and produce resonant modes into which the trigger can couple.

[41] A readily distinguishable low-frequency component was also not observed for relatively small slug sizes ($L' < 5$, Figure 12b), presumably either as a result of the weakness of the excitation process or an absence of suitable conditions to sustain the oscillation. For larger slug sizes, the low-frequency component shows a systematic decrease in frequency with increasing slug length, and the high-viscosity data consistently plot at lower values than the low-viscosity data. In order to assess the validity of our hypothesis that this component represents an oscillation of the gas slug remaining in the lower tube, we use the formula for the longitudinal oscillation of liquid "bouncing" on a gas slug [*Vergniolle et al.*, 1996]:

$$f_L = \frac{1}{2\pi}\sqrt{\frac{\gamma P_g}{\rho L_{eq} H_l}}, \tag{7}$$

which was successfully used to model gliding experimental pressure oscillations by *James et al.* [2004]. Here, γ is the ratio of specific heats of the gas ($\gamma = 1.3$ for air), L_{eq} is the equilibrium bubble length, H_l is the depth of the slug in the liquid, ρ is the liquid density and P_g is the gas pressure in the slug. Figure 12c compares the experimental data with equation (7), in which we use $P_g = 105$ kPa, $\rho = 1000$ or 1250 kg m^{-3} and L_{eq} is expressed in terms of slug aspect ratio. L_{eq} values are calculated as the original slug aspect ratio (given on the abscissa) minus 3.3 – the approximate "size" of the first bubble produced when the slug is disrupted in the flare - and hence represent the sizes of the gas slugs remaining in the lower tube after the first liquid piston has formed. For each viscosity, a value of H_l is obtained that provides a best fit model to the data. In equation (7), the values of H_l correspond to liquid depths within a tube with the same diameter as the gas slug. To account for the flare in our application, we convert these values into equivalent liquid depths in the larger-diameter tube, to yield depths of 0.05 m (0.001 Pa s) and 0.06 m (0.1 Pa s). The reasonable model fits displayed in Figure 12c support the hypothesis that these low-frequency signals originate in the natural frequency oscillations of a constant "active volume" of liquid perched on the portion of the gas slug remaining in the lower tube. An indication of the sensitivity of this analysis can be obtained by assuming alternative values of H_l. The dashed lines in Figure 12c are

Figure 12. (a) Amplitude and (b) frequency of fluid-driven oscillatory pressure changes recorded at ASG 4 during the ascent of gas slugs through a flare with 1:4.4 area change ratio, separated into high- and low-frequency components. Only experiments carried out in intermediate- (0.1 Pa s) and low-viscosity (0.001 Pa s) liquids produced results suitable for comparison, and these results are plotted as functions of the equivalent slug aspect ratio L' (see equation (5)) of the slug in the lower, smaller tube. In Figure 12a, each symbol represents an average of five experiments and, where the range of the data exceeds the symbol size, this range is given by the error bars. The dashed line portions of the plot in Figure 12a represent data for which a dominant frequency component was not observable (see Figure 12b), and the pressure change for these cases represents a maximum amplitude within suitably band-passed data. (c) Comparison of low-frequency component data (key as for Figure 12a) with a slug oscillation model. Black curves are for 0.001 Pa s data, and gray curves are for 0.1 Pa s data. For the frequency data the solid curves show best fit results. Model results assuming much larger (dotted curves) or smaller (dashed curves) oscillating liquid volumes (see text for details) are also shown for comparison with best fits. (d, e) Pressure recorded at ASG 1 illustrating the repeatability of longer-period components ($\sim$0.5 s) of pressure changes between experiments and steady variation of pressure changes with slug size and liquid viscosity, μ. Superimposed data from five repeat experiments for each slug aspect ratio have been band-passed between 1 and 8 Hz to remove signals due to apparatus oscillation. Different slug aspect ratios are vertically offset for clarity.

results obtained for a depth of 0.04 m, representing the approximate height of liquid in the lower tube which is above the remainder of the gas slug, while the dotted lines are results for a depth of 1.33 m, equivalent to the full volume of the liquid in the upper, larger tube. Neither of these depths provides a reasonable fit to the data. The size of the "active volume" is likely to be determined by the absolute and relative sizes of the tubes on either side of the flare, as well as the fluid properties. For the liquids used here, viscosity does not appear to have a significant influence on the size of the "active volume" and the number of oscillatory cycles observed (1–3) provides a timescale over which the resonant fluid distribution is stable. Note, however, that this model does not take into account the presence of the overlying bubble and is thus significantly simpler than the real scenario.

[42] A further test of the applicability of this model is to also consider the amplitude of the pressure oscillations. The potential energy, E_p, for small oscillations of a gas spring is given by *Vergniolle et al.* [1996] as

$$E_p = \frac{1}{2}\left[\frac{\pi R^2 \gamma P_g}{L_{eq}}\right](\Delta L)^2, \tag{8}$$

where R is the radius of the gas spring ($R \approx 1/2D$) and ΔL is the length change during oscillation, which, assuming an ideal gas, is proportional to the peak-to-peak magnitude of the pressure change in the slug. The smooth upper curves in Figure 12c are fits of this equation to the ASG 4 data (for $L' > 5$) based on optimal values for E_p (0.023 J for 0.001 Pa s and 0.016 J for 0.1 Pa s). For $L' < 3.3$, the curves cannot be made to fit the data and the model is not applicable, in agreement with observations that there is no slug disruption below the flare. For $3.3 < L' < 5$, we assume that the "gas spring" model is inadequate to fully represent the complex situation when only a relatively small volume of gas is involved or the appropriate value of E_p has changed. Therefore both frequency and amplitude data are consistent with the "bouncing" of an "active volume" of liquid on a gas spring.

[43] It is interesting to note that a particular pressure transient or frequency component could not be directly attributed to the jet-like ascent of the bubble nose, observed shortly after slug disruption. With the upward flux of gas being necessarily matched by a volumetrically equivalent downward flux of liquid, significant pressure changes would intuitively be expected during this process. We hypothesize that the timescale over which this occurs (~0.2 s) is too similar to the period of the low-frequency component of pressure oscillation to enable these processes to be identified individually. It is possible that the first oscillation of the low-frequency component of pressure is related to the jet-like bubble ascent process or, alternatively, that the jet-like ascent is induced by pressure changes from the underlying slug oscillation. Band-passed pressure data from ASG 1 (Figures 12d and 12e) point to the presence of further, longer-period (~0.3–0.7 s), low-magnitude (~1 kPa) pressure changes. These timescales are too long to be directly resulting from the interval of jet-like ascent, but rather are believed to reflect overall pseudo-static pressure changes, and hence give a global indication of the period during which the slug transition through the flare occurs. Figures 12d and 12e also further emphasize the repeatability of the events and demonstrate how parameters such as relative slug lengths could be obtainable from the data.

[44] Experiments carried out with different heights of liquid above the widening (up to ~0.6 m) did not display strong variations in the overall magnitude of the pressure change or dominant frequency of the source, when the liquid level was greater than approximately one diameter deep in the upper tube (Figure 13a). This supports the previous suggestion of an effectively constant "active volume" that has approximately equal depth and diameter. However, detailed observation of data band-passed in order to isolate the low- and high-frequency components does indicate some changes when the liquid depth is less than 0.3 m (Figures 13b–13e). Note that initial source transients remain robust, although the waveforms diverge at later times.

3.2.6. Process Overview

[45] Our interpretation of the sequence of events responsible for exerting net vertical forces on the apparatus during slug breakup precipitated by a flare and under inertially dominated conditions (Figure 5), is, therefore, as follows.

[46] 1. As the slug nose enters the flare, the change in the liquid flow field around it induces a small-magnitude upward force on the apparatus (Figures 8, 9, and 11a).

[47] 2. The slug nose expands horizontally into the wider-diameter tube and an increasing liquid flux begins to flow into the top of the smaller tube, forming a narrowing neck in the slug (Figure 5).

[48] 3. This process continues until the narrowing slug neck finally closes (Figure 5a, sketch v), temporarily halting the upward flow of gas into the flare. The point of closure acts as an impulsive trigger mechanism, which produces a substatic pressure above it, and a superstatic pressure pulse below (Figure 11e).

[49] 4. Coupling of the substatic fluid pressure to the apparatus at the flare accelerates the apparatus upward (Figure 11e).

[50] 5. When the downward-traveling superstatic pressure wave reaches the base of the tube, the apparatus accelerates downward (Figure 11e). The initial upward distance traveled by the apparatus reflects the magnitude of the pressure decrease in the flare and the time taken for the high-pressure pulse to reach the base.

[51] 6. These pressure perturbations stimulate a longitudinal standing wave within the fluid column (the acoustic high-frequency component of the pressure signal in Figures 5c, 11b, and 11c), which is terminated as the gas distribution changes over the timescale of one cycle.

[52] 7. At the closure of the narrowing slug neck in (3), the liquid involved forms a downward-moving liquid "piston," which then decelerates on the gas spring represented by the remainder of the slug in the small tube. Ensuing longitudinal slug/piston oscillations appear to be manifested in the low-frequency inertial component of the pressure oscillations (Figures 11b and 11c). These are terminated as the remainder of the slug ascends into the flare.

3.3. Tube Bulge

[53] Experiments were also carried out using a combination of widening and narrowing elements with a length-

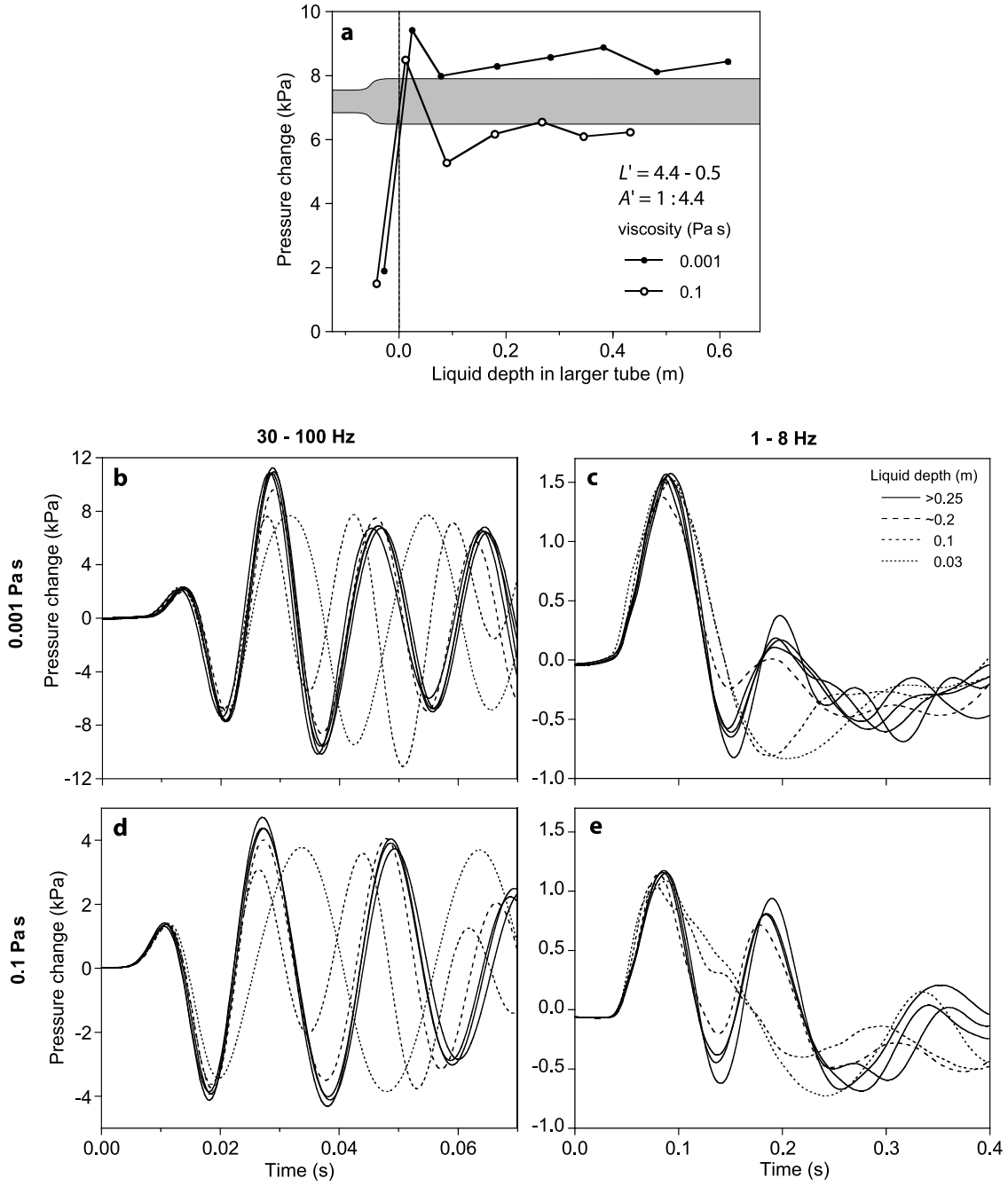

Figure 13. Pressure changes as a function of liquid depth for a slug ascending through a flare. (a) The amplitude of the maximum pressure change recorded at ASG 1 at the base of the apparatus varies little once the liquid depth is greater than approximately one tube diameter (marked by the vertical dotted line). The scaled gray image demonstrates the tube geometry relative to the plot data. (b–e) More subtle pressure variations are displayed by band-passed ASG 4 data. The solid lines represent data (averages of five experiments each) for liquid depths of ~0.25 m and greater. The long-, intermediate-, and short-dashed lines show data for liquid depths of ~0.2, 0.1, and 0.03 m, respectively, corresponding to the symbols in Figure 13a. Systematic variation of the pressure traces with liquid depth are observed in the data collected for these "shallow" liquid depths.

limited segment of enlarged tube in between. The observed flow patterns can be described as sequences of the above documented processes. When slugs were disrupted within the flare, the resulting bubbles then coalesced within the diameter reduction. Varying the distance between the regions of diameter change did not appear to have a significant influence on the flow processes observed.

[54] Examples of pressure traces obtained in experiments with back to back concentric reducers - the shortest length bulge used - are shown in Figure 14. For long slugs flowing

through small changes in diameter, pressure changes characteristic of the slug nose entering the expansion (Figure 14b, 1.9 s; compare with Figure 8a, 1.8 s), slug flowing up the wider section (Figure 14b, 2.5–2.8 s), and slug gradually entering back into the narrower tube (Figure 14b, 2.8–3.6 s; compare with Figure 4b, 1.5–2.0 s) were recorded. For severe changes in tube diameter (area ratio 1:4.4), pressure oscillations displayed amplitudes and frequencies similar to those observed for a tube widening (compare Figures 8c and 14c), with the effects of the tube narrowing being small on this scale. Therefore both physically and fluid dynamically, the bulge can be considered to comprise a tube widening followed by a tube narrowing. Note the absence of any static pressure offset in Figure 14, unlike those observed in Figures 4 and 8–10, due to the slug geometry being identical above and below the bulge discontinuity.

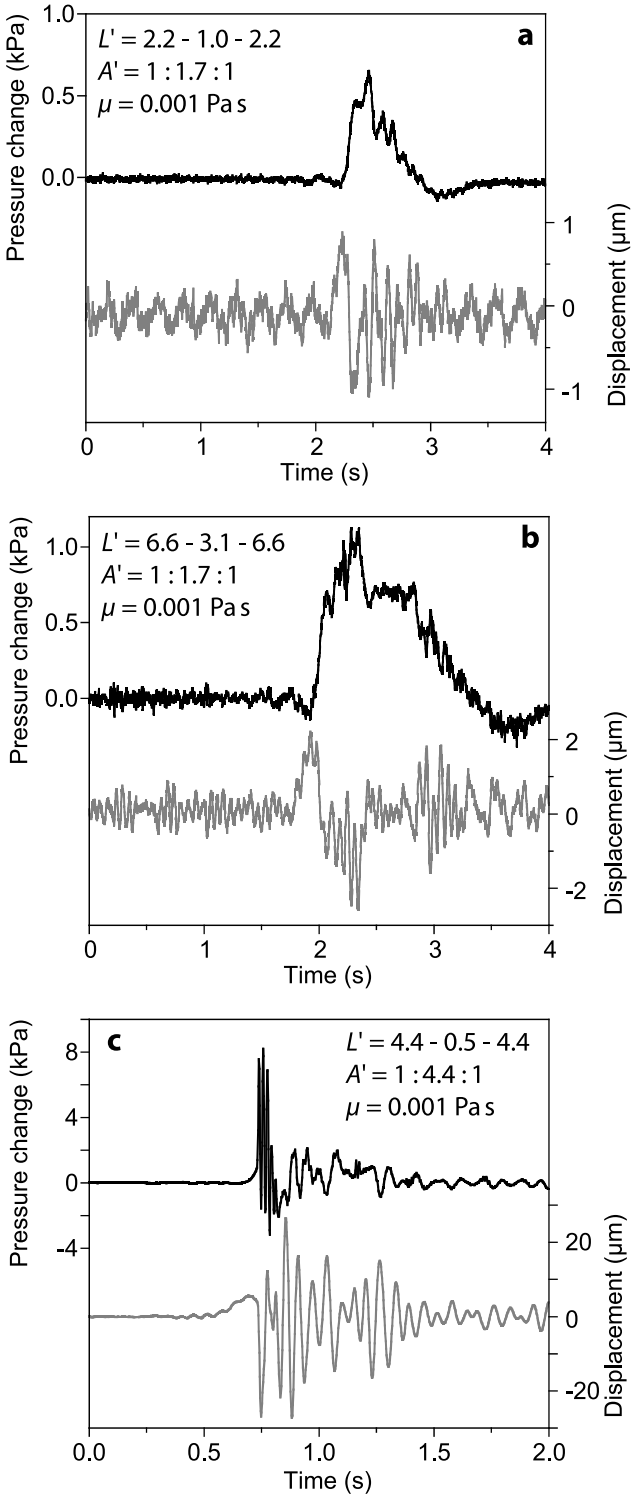

Figure 14. Pressure at ASG 1 (black traces) and apparatus displacement (gray traces) recorded during slug ascent through segments of wider tubes (juxtaposed flares and inverted flares) in 0.001 Pa s viscosity liquid. Equivalent slug aspect ratios are given in each plot for reference; however, note that stable slug ascent within the short, wider section did not fully develop. (a) Results for a small slug traversing a region of slightly wider diameter tube. (b) Results for a longer slug ascending the same tube geometry as in Figure 14a. (c) Results for an intermediate-length slug traversing a limited region of significantly wider tube.

[55] Changes in the vertical separation distance between the two bulge shoulders did not result in any significant differences in the pressure amplitudes recorded (Figures 15a and 15c). This is consistent with an "active volume" of approximately equal height and diameter. However, shorter bulges could not be investigated due the physical nature of the concentric reducers used in the apparatus, which constrained effective bulge lengths to be equal to, or larger than the bulge diameter (Figure 1b). Consequently, the "active volume" was always smaller than the bulge volume.

[56] For more detailed comparisons of the low- and high-frequency components, band-passed ASG 4 data are given in Figures 15a and 15c. The high-frequency components (acoustic resonance within the liquid column) from the different tube geometries are indistinguishable (Figure 15a), indicating that this component is affected little by geometry above the widening bulge shoulder. For the low frequencies (Figure 15c), onsets remain very similar, suggesting that source processes between bulges and single flares are related. Following the signal onsets in Figure 15c, differences emerge between the signals with higher pressures for the bulge configuration. This may not be surprising if large-scale motion of gas and liquid above the flare is indeed their source.

[57] In contrast to the pressure data, comparison of apparatus displacements point to significantly reduced apparatus oscillations generated by slug propagation through a bulge, e.g., an amplitude of ~25 μm in Figure 14c, compared with an amplitude of ~85 μm in Figure 8c for a single flare. Band-passed apparatus accelerations are shown in Figure 15b and 15d. As the corresponding pressure magnitudes are similar during these experiments, the differences in recorded accelerations between bulge and flare configurations point to the importance of tube geometry in determining how the pressure changes couple to the apparatus to drive apparatus motion. The apparatus is moved upward by superstatic pressure pulses coupling to downward-facing tube wall, and substatic pressure pulses coupling to upward-facing tube wall. Downward motion results from substatic pressure pulses acting on downward-facing wall, and superstatic pressure pulses on upward-

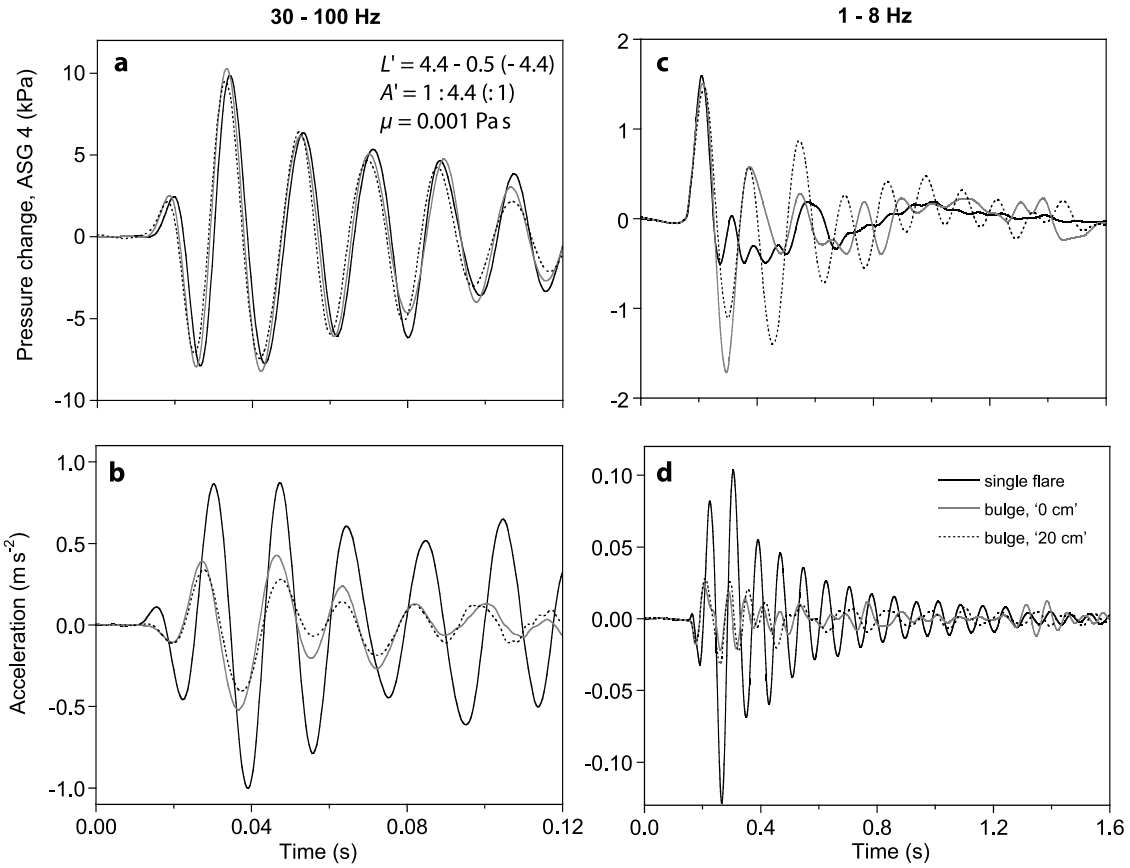

Figure 15. Comparison of high- and low-frequency components of pressure changes produced by slug ascent through single flares and length-limited expansions (bulges) in water. Each trace represents the band-passed result of data averaged from five experiments. Solid black lines are data for a single flare with area ratio 1:4.4. Solid gray lines represent data for a short length-limited expansion obtained by juxtaposing a flared section with area ratio 1:4.4 (Figure 1b) with an identical, but inverted (A' = 4.4:1), flared section. Dashed black lines show data from a similar tube geometry, but with a 0.2 m long section of 0.08 m diameter tube separating the flare and inverted-flare sections. Data have been band-passed to display the (a, b) high-frequency and (c, d) low-frequency components of ASG 4 pressure (Figures 15a and 15c) and apparatus acceleration, $\ddot{s}_z$ (Figures 15b and 15d). Pressure changes are very similar for all tube geometries, with length-limited bulge segments providing extended low-frequency oscillations. In contrast, apparatus accelerations differ significantly, with much greater accelerations being produced by the single flare geometry. Note also that the onset of the high-frequency component of acceleration is upward for the single flare and downward for the length-limited expansions.

facing wall. In the case of a symmetrical bulge the forces applied to the tube cancel out, leaving only the dynamic pressure acting on the base to move the apparatus. Therefore the apparatus motion is expected to be less for the bulge than for the flare.

4. Volcano-Seismic Implications

[58] To assess the implications of the laboratory slug disruption dynamics (summarized in Table 1) for volcanic processes inferred from seismic data, laboratory observations must be scaled to relevant field values. However, due to the transient nature of the observed processes, traditional scaling arguments based on dimensionless numbers cannot be rigorously applied. Initially, it should be determined whether significant liquid accelerations or decelerations are to be expected, or whether the transient-free and oscillation-free results observed in high-viscosity experiments (~30 Pas) represent a more relevant scenario. With no direct scaling for the geometry change transition, we consider the dimensionless parameters provided for steady state slug ascent in the different-sized tubes or conduits (Table 2) in order to ascertain the likelihood of significant transients being produced. In the laboratory case, the low viscosity of water ensures that slug flow in both small and large pipes is inertially controlled. No significant differences exist between the flow-defining parameters for either sized pipe. In the volcanological case, the effect of higher-viscosity silicate melt is reflected in significantly smaller inverse viscosity (N_f) values compared to water (Table 2). This suggests that liquid accelerations, and hence, seismically measurable forces, might be reduced. Although this indicates that in a 2-m-diameter tube slug ascent is controlled by both inertial and viscous forces ($Fr < 0.345$, $N_f <$

Table 1. Summary of Experimental Findings Under Inertaly Dominated Conditions

Conduit Diameter Change	Slug Velocity Change	Flow Regime Change	Liquid Accelerations	Pressure Oscillations	Apparatus Motion
Increase	increase	Can be significant; disruption of slug into multiple bubbles; generation of transient jetting.	Large, associated with magnitude of flow regime change; rapid decelerations of liquid involved in slug disruption.	Significant when slug is disrupted into different bubbles.	Significant, but depends on details of where pressure oscillation couples to tube wall.
Decrease	decrease	Minimal; inertial effects reduced, viscous control enhanced; small trailing bubbles may coalesce with slug base.	Minimal; changes associated with adjustment of the flow field around the slug nose to the reduced diameter conduit.	Generally small, complex oscillations generated if the falling liquid film around the new, longer and narrower slug becomes unstable.	Minimal.

200), in a 5-m-diameter tube, inertial effects dominate ($Fr \approx 0.345$, $N_f > 200$). If the relevant process to be considered is rapid liquid flow from the larger pipe into the smaller one, then the increasing relative importance of viscosity within the smaller pipe could possibly enhance rather than reduce the likelihood of significant transient effects.

[59] For an estimation of the magnitude of the forces produced, we perform an order of magnitude calculation using simple geometric estimates. In our experiments, net forces on the apparatus can be estimated by considering the recorded vertical accelerations. Acceleration amplitudes of up to 1 m s^{-2} were recorded (e.g., Figures 2 and 11d), which, for the apparatus mass of ~30 kg, imply forces of up to ~30 N. On the basis of our interpretation of the experimentally generated force being the result of the deceleration of a volume of liquid, one may then estimate the equivalent volcanological force by scaling the liquid mass by both density and volume (or cubic length). Given that silicate magmas are roughly two to three times denser than water, and also that volcanic conduit dimensions are approximately two orders of magnitude larger than the laboratory tube dimensions, the scaling factor is $\sim 2.5 \times 10^6$. Applying this to the observed force of 30 N suggests that a force of 10 to 100 MN could be realized in a volcanological system. If this acted along a conduit 2 m in diameter, it would imply pressure increases of order 1–10 MPa. As this analysis does not account for the viscosity or compressibility of bubbly magma, it is likely to represent maximum values. Nevertheless, it demonstrates that the processes observed in our experiments may be capable of generating similar magnitude forces and pressures to those required by *Chouet et al.* [2003] to explain their VLP data from Stromboli and similar pressures to those suggested by *Vergniolle* [1998] from acoustic data recorded at Stromboli. No other previously suggested process (e.g., foam collapse, slug ascent up straight conduits) has been demonstrated capable of producing pressures and forces of such magnitudes without requiring an initial (and unaccounted for) overpressure at depth.

[60] For further insights, the oscillation periods involved can be considered, which, for VLP events, are some 50 times longer than the periods of laboratory pressure oscillations, due to the larger conduit dimensions and greater magmatic fluid volumes. *Vergniolle et al.* [1996] demonstrated that longitudinal oscillations of gas slugs near the surface at Stromboli could explain acoustic frequencies of 0.5–1 Hz. Here, we examine whether applying a similar model for slug disruption could produce reasonable parameters for the seismic events generated at depths of 220 and 260 m as recorded by *Chouet et al.* [2003].

[61] Should the VLP seismic signals at Stromboli result from a process equivalent to a liquid piston bouncing on a gas spring, then the work done to compress the gas can be equated to the potential energy lost by a magma column of height H and cross sectional area A, assumed to fall a distance s, before coupling to the gas. For an order of magnitude estimate we assume an isothermal ideal gas behavior so that the work done during compression is given by the product of the mean force (1/2 (final overpressure - initial overpressure) $\times$ A) times compression distance. Accordingly, for a gas pressure increase ΔP_g resulting from a gas volume decreasing only along its initial vertical dimension L_{eq}, by an amount ΔL, we obtain

$$\frac{1}{2}\Delta P_g A \Delta L = \rho g H A (s + \Delta L). \quad (9)$$

Table 2. Dimensionless Parameter Values for Slug Flow in the Laboratory and in Volcanoes

	Laboratory Scale[a]		Field Scale[b]	
	D = 0.038 m	D = 0.08 m	D = 2 m	D = 5 m
Fr	(a) 0.35; (b) 0.34; (c) 0.01	(a) 0.35; (b) 0.35; (c) 0.04	0.23	0.34
Mo	(a) 10^{-11}; (b) 10^{-3}; (c) 10^7	(a) 10^{-11}; (b) 10^{-3}; (c) 10^7	10^9	10^9
Eo	(a) 200; (b) 250; (c) 270	(a) 900; (b) 1100; (c) 1200	10^5	10^6
N_f	(a) 10^4; (b) 290; (c) 1	(a) 10^5; (b) 900; (c) 3	60	228

[a] σ = 0.07 N m^{-1}; (a) μ = 0.001 Pa s, ρ = 1000 kg m^{-3}; (b) μ = 0.1 Pa s, ρ = 1250 kg m^{-3}; (c) μ = 30 Pa s, ρ = 1340 kg m^{-3}; area ratio, A' = 1:4.4.
[b] σ = 0.4 N m^{-1}; μ = 400 Pa s, ρ = 2600 kg m^{-3}; area ratio, A' = 1:6.3.

Furthermore, $\Delta L = L_{eq}\Delta P_g/(P_g + \Delta P_g)$, and (with $\gamma = 1$) equation (7) can be rearranged for H, to give

$$H = \frac{P_g}{(2\pi f_L)^2 \rho L_{eq}}. \quad (10)$$

This allows equation (9) to be formed as a quadratic equation in L_{eq}:

$$\frac{2\pi^2 f_L^2}{g} L_{eq}^2 - \frac{P_g}{\Delta P_g} L_{eq} - \frac{P_g(P_g + \Delta P_g)}{\Delta P_g^2} s = 0, \quad (11)$$

in which only positive roots represent relevant solutions.

[62] Values for ΔP_g are currently poorly constrained by field measurements, so we consider two end-member scenarios. First, a minimum value of ΔP_g may be obtained by considering the volume change associated with the initial dike inflation phase calculated by *Chouet et al.* [2003] ($\sim$100 m^3). Assuming a penny-shaped dike with radius $a \approx 100$ m requires an average aperture increase, Δw, of 0.3 cm to account for a volume expansion of 100 m^3. For a penny-shaped crack subjected to a uniform distribution of internal pressure, the excess pressure, ΔP, necessary to produce this expansion, is given by [*Sneddon and Lowengrub*, 1969]

$$\Delta P = \frac{3\pi}{4a}\left(\frac{\mu(\lambda + \mu)}{\lambda + 2\mu}\right)\Delta w, \quad (12)$$

where λ and μ are the Lamé coefficients of the rock matrix. Assuming $\lambda = 2\mu$ with elastic shear modulus $\mu = 7$ GPa [*Chouet et al.*, 2003], we obtain $\Delta P = 0.4$ MPa. Note that this approach may significantly underestimate the excess pressure in the process envisioned at Stromboli, which may be more accurately described by a pressure transient applied over a small patch of crack wall in a vertical fluid-filled crack open to the surface and under an initial static gradient of pressure.

[63] As an alternative approach, a maximum value of ΔP_g may be estimated from the $\sim$100 MN downward-acting single force calculated by *Chouet et al.* [2003]. Assuming that this force is the result of an isotropic source of excess pressure applied at depth within a nearly enclosed system, then ΔP_g can be calculated by estimating the liquid free surface area over which the pressure did not couple into the surrounding rock. This may be taken as the cross sectional area of the vent or cross sectional area of the dike imaged at Stromboli if the liquid level is sufficiently low. Choosing a value between 10 and 100 m^2 (representing a vent radius of $\sim$2–6 m or a dike with aperture of 1 m and width 10–100 m) yields $\Delta P_g \approx 1$–10 MPa. This approach is again limited by the fact that the dynamics associated with the event are not represented and any complications in sub-liquid surface geometry are neglected.

[64] Assuming the upper 20 m of the conduit are magma-free, with $\rho = 2600$ kg m^{-3} we obtain $P_g = 5.1$ MPa for a magma depth of 200 m, or $P_g = 6.1$ MPa for a magma depth of 240 m. Our experiments suggest that appropriate values of s are on the order of the (upper) tube diameter. Using $s = 1$ m appropriate for a dike aperture at Stromboli, and $f_L \approx 0.3$ Hz derived from Figures 9 and 10 of *Chouet et al.* [2003], we obtain $L_{eq} \sim 80$ m for $\Delta P_g = 0.4$ MPa, and $L_{eq} \sim 3.5$ m for $\Delta P_g = 10$ MPa. Slug lengths of a few tens of meters are plausible (and have been estimated from acoustic measurements at Stromboli [*Vergniolle et al.*, 1996]), suggesting that slug disruption is a possible mechanism for exciting shorter-period ($\sim$3 s) components of the VLP signals observed at Stromboli by *Chouet et al.* [2003]. The corresponding heights of the "active volume" are 6 and $\sim$140 m respectively, which would represent masses of 50–1100 tons. Unlike our experiments, where the active volumes appeared to be relatively equant, these suggested heights are significantly larger than the assumed dike aperture. Although this may indicate that the slug breakup mechanism is not applicable to Stromboli, the details of the physical process of slug breakup are difficult to assess for a dike-like conduit geometry and, given the rough nature of these estimates, we tentatively conclude that this particular process cannot be rejected a priori. Invoking the slug disruption mechanism for periods appropriate to the LP band (0.3–1 s) would imply slug lengths of $\sim$0.3–15 m and associated oscillating masses of $\sim$10–600 tons.

[65] For the longest periods (15 s) of the VLP events recorded by *Chouet et al.* [2003], slug lengths of $\sim$1000 m are required for small values of ΔP_g, although for $\Delta P_g = 10$ MPa slug lengths of $\sim$50 m are implied. These results suggest that both LP and VLP sources could result directly from the slug disruption mechanism under appropriate conditions. However, this would require large dynamic overpressures to explain the longest-period signals. Alternatively, the longest-period components of VLP events at Stromboli [*Chouet et al.*, 2003, Figure 3] may originate in mechanisms that are distinct from those generating the shorter-period ($\sim$3 s) components. If the 3 s period components are due to slug disruption, the longer periods could represent the overall timescale of the slug transition through the geometry change, as indicated in Figures 12d and 12e. The absence of 15 s period components in type 1 events at Stromboli [e.g., *Chouet et al.* 2003, Figure 3] may signify the proximity of the liquid surface to the discontinuity, in which case bursting of the bubble or slug would curtail the duration of the signal and mask other pseudo-static pressure changes. These conditions are represented in experiments where the liquid surface was so low that the bubble nose reached the surface during the period of jet-like ascent. In these cases, bubble burst was usually associated with an audible "pop" and liquid droplets being propelled $\sim$0.5 m up the tube, representative of a significantly more energetic event than "normal" slug bursts. Similarly, at Stromboli, the type 1 events (without a 15 s VLP component) were associated with "cannon-like blasts" a few seconds long, in contrast to type 2 events which were much less impulsive and lasted longer (up to 20 s) [*Chouet et al.*, 2003]. This is also in harmony with the relative source depths ascertained by *Chouet et al.* [2003], which suggest that the centroid of type 2 events is $\sim$40 m deeper than that of type 1 events.

[66] Our canonical apparatus geometry may be relatively representative of conduits entering lava lakes but is expected to be very much simplified with respect to most other relevant volcanological settings, where generally dike-like geometries are envisaged. In spite of such limitations, our experiments demonstrate pressure and single-force events that are scalable in magnitude, and similar in

repeatability, to seismic sources recorded at low magmatic-viscosity volcanoes [*Rowe et al.*, 1998, 2000; *Aster et al.*, 2003; *Chouet et al.*, 2003]. The process of small-volume liquid slumping and rapid liquid deceleration (in particular when this process occurs during the breakup of slugs in severe conduit diameter expansions) has been shown to be a viable seismic source. We anticipate that this general mechanism is likely to operate over a wide range of severe geometry change styles and therefore could be responsible for VLP and LP events in many other scenarios as well as slug flow into lava lakes. We thus propose the rapid deceleration of downward-moving liquid as an alternative interpretation of the source of some pressures and forces currently attributed in volcano-seismic analyses to represent slower, upward accelerations of much larger liquid volumes. Provided equivalent seismic events can be recorded, increased understanding of the fluid flow mechanisms involved may allow parameters such as conduit geometry and slug size to be recoverable from VLP seismic data.

[67] The complex spatial distributions of pressure changes demonstrated in our experiments underscore the requirement for detailed analyses of source space-time functions (including both moment-tensor and single-force components) of relevant seismic data. Our experiments emphasize the importance of conduit geometry, not only in initiating transient fluid flow events, but also in dictating how (and where) pressure fluctuations couple into the confining medium as single forces. This is particularly apparent in the ''bulge'' geometry, where pressure transients are larger but apparatus accelerations are smaller than in flares, due to the axial symmetry in the tube geometry. For our experiments, examining bulk fluid momentum changes alone (as considered by current seismic analyses done on point sources) would not yield the details necessary to reconstruct the overall source process. The single forces recorded are a function of both the pressure changes induced in the fluid and the timing of when these changes couple into the apparatus. Consequently, apparatus motion depends not only on when pressure changes are generated, but also on the relative positions of the source and force-coupling locations, as well as the effective sound speed of the fluid between these sites. Hence inversions of seismic waveforms may need to be carried out over a spatially extended source, rather than a point source, in order to fully express the source dynamics.

5. Conclusions

[68] The ascent of gas slugs through changes in tube diameter generates a wide variety of complex pressure changes. Severe increases in diameter can induce the breakup of slugs and are responsible for the largest-amplitude pressure signals. Where viscous control is dominant, rapid pressure increases and slower decreases occur during slug breakup, but the net forces generated are negligible. In liquids where viscosity does not completely dominate flow processes and fluid inertia is important, rapid momentum changes in the liquid induce single forces on the confining tube. Slug flow through conduit geometry changes could, therefore, be responsible for the single-force components of the VLP seismic signals produced by Strombolian explosions. However, it may be critical to consider how, when and where, fluid momentum changes couple to the conduit in order to fully understand single-force components. In contrast to previous work (in which pressures and downward forces on conduits have been attributed to relatively slow upward acceleration of large liquid masses), during slug disruption in conduit flares the greatest pressures and downward forces are generated by the rapid deceleration of small volumes of downward-moving liquid.

[69] The repeatability of recorded pressure data, and dependence of the magnitude of the pressure transient on parameters such as slug size, suggest that more direct links between moment-tensor and single-force representation of seismic sources and fluid flow processes are not only possible, but could potentially provide a wealth of information not available from seismic data alone. These results provide strong support for further experiments covering more styles of geometry change and continued inversions of relevant seismic data for more detailed source representations.

[70] **Acknowledgments.** This work was funded by The Royal Society and the Leverhulme Trust. We thank L. Wilson for valuable discussions and improvements to the text of this paper. S. Vergniolle and an anonymous reviewer and Associate Editor are thanked for their constructive reviews.

References

Aloui, F., L. Doubliez, J. Legrand, and M. Souhar (1999), Bubbly flow in an axisymmetric sudden expansion: Pressure drop, void fraction, wall shear stress, bubble velocities and sizes, *Exp. Therm. Fluid Sci.*, *19*, 118–130.

Aster, R., S. Mah, P. Kyle, W. McIntosh, N. Dunbar, J. Johnson, M. Ruiz, and S. McNamara (2003), Very long period oscillations of Mount Erebus Volcano, *J. Geophys. Res.*, *108*(B11), 2522, doi:10.1029/2002JB002101.

Bruce, P. M., and H. E. Huppert (1989), Thermal control of basaltic fissure eruptions, *Nature*, *342*, 665–667.

Chouet, B., P. Dawson, T. Ohminato, M. Martini, G. Saccorotti, F. Giudicepietro, G. De Luca, G. Milana, and R. Scarpa (2003), Source mechanisms of explosions at Stromboli Volcano, Italy, determined from moment-tensor inversions of very-long-period data, *J. Geophys. Res.*, *108*(B1), 2019, doi:10.1029/2002JB001919.

Chouet, B., P. Dawson, and A. Arciniega-Ceballos (2005), Source mechanism of Vulcanian degassing at Popocatépetl Volcano, Mexico, determined from waveform inversions of very long period signals, *J. Geophys. Res.*, *110*, B07301, doi:10.1029/2004JB003524.

Clift, R., J. R. Grace, and M. E. Weber (1978), *Bubbles, Drops and Particles*, Elsevier, New York.

Deshpande, N. S., and M. Barigou (2001), Foam flow phenomena in sudden expansions and contractions, *Int. J. Multiphase Flow*, *27*, 1463–1477.

Dimakopoulos, Y., and J. Tsamopoulos (2003a), Transient displacement of a Newtonian fluid by air in straight or suddenly constricted tubes, *Phys. Fluids*, *15*, 1973–1991.

Dimakopoulos, Y., and J. Tsamopoulos (2003b), Transient displacement of a viscoplastic material by air in straight and suddenly constricted tubes, *J. Non Newtonian Fluid Mech.*, *112*, 43–75.

Fabre, J., and A. Liné (1992), Modelling of two-phase slug flow, *Annu. Rev. Fluid Mech.*, *24*, 21–46.

Founti, M., T. Achimastos, and A. Klipfel (1999), Effects of increasing particle loading in an axisymmetric, vertical, liquid-solid sudden expansion flow, *J. Fluids Eng.*, *121*, 171–178.

Gutmundsson, A. (2005), The effects of layering and local stresses in composite volcanoes on dyke emplacement and volcanic hazards, *C. R. Geosci.*, *337*(13), 1216–1222.

James, M. R., S. J. Lane, B. Chouet, and J. S. Gilbert (2004), Pressure changes associated with the ascent and bursting of gas slugs in liquid-filled vertical and inclined conduits, *J. Volcanol. Geotherm. Res.*, *129*, 61–82, doi:10.1016/S0377-0273(03)00232-4.

Jaupart, C., and S. Vergniolle (1989), The generation and collapse of a foam layer at the roof of a basaltic magma chamber, *J. Fluid Mech.*, *203*, 347–380.

Kieffer, S. W. (1977), Sound speed in liquid-gas mixtures: Water-air and water-steam, *J. Geophys. Res.*, *82*, 2895–2904.

Kirchdörfer, M. (1999), Analysis and quasistatic FE modeling of long period impulsive events associated with explosions at Stromboli Volcano (Italy), *Ann. Geofis.*, *42*, 379–390.

Kumagai, H., B. A. Chouet, and M. Nakano (2002), Waveform inversion of oscillatory signatures in long-period events beneath volcanoes, *J. Geophys. Res.*, *107*(B11), 2301, doi:10.1029/2001JB001704.

Lin, J., and J. P. Gollub (1994), Solitary wave dynamics of film flows, *Phys. Fluids*, *6*, 1702–1712.

Neuberg, J., R. Luckett, M. Ripepe, and T. Braun (1994), Highlights from a seismic broadband array on Stromboli volcano, *Geophys. Res. Lett.*, *21*, 749–752.

Ohminato, T., B. A. Chouet, P. Dawson, and S. Kedar (1998), Waveform inversion of very long period impulsive signals associated with magmatic injection beneath Kilauea Volcano, Hawaii, *J. Geophys. Res.*, *103*, 23,839–23,862.

Poole, R. J., and M. P. Escudier (2003), Turbulent flow of a viscoelastic shear-thinning liquid through a plane sudden expansion of modest aspect ratio, *J. Non Newtonian Fluid Mech.*, *112*, 1–26.

Ripepe, M., and E. Gordeev (1999), Gas bubble dynamics model for shallow volcanic tremor at Stromboli, *J. Geophys. Res.*, *104*, 10,639–10,654.

Ripepe, M., S. Ciliberto, and M. Della Schiava (2001), Time constraints for modeling source dynamics of volcanic explosions at Stromboli, *J. Geophys. Res.*, *106*, 8713–8727.

Rowe, C. A., R. C. Aster, P. R. Kyle, J. W. Schlue, and R. R. Dibble (1998), Broadband recording of Strombolian explosions and associated very-long-period seismic signals on Mount Erebus volcano, Ross Island, Antarctica, *Geophys. Res. Lett.*, *25*, 2297–2300.

Rowe, C. A., R. C. Aster, P. R. Kyle, R. R. Dibble, and J. W. Schlue (2000), Seismic and acoustic observations at Mount Erebus volcano, Ross Island, Antarctica, 1994–1998, *J. Volcanol. Geotherm. Res.*, *101*, 105–128.

Seyfried, R., and A. Freundt (2000), Experiments on conduit flow and eruption behavior of basaltic volcanic eruptions, *J. Geophys. Res.*, *105*, 23,727–23,740.

Sneddon, I. N., and M. Lowengrub (1969), *Crack Problems in the Classical Theory of Elasticity*, John Wiley, Hoboken, N. J.

Sommerfeld, M., A. Ando, and D. Wennerberg (1992), Swirling, particle-laden flows through a pipe expansion, *J. Fluids Eng.*, *114*, 648–656.

Taha, T., and Z. F. Cui (2006), CFD modelling of slug flow in vertical tubes, *Chem. Eng. Sci.*, *61*, 676–687.

Vergniolle, S. (1998), Modelling two-phase flow in a volcano, paper presented at 13th Australasian Fluid Mechanics Conference, Aristoc. Offset, Monash Univ., Melbourne, Australia.

Vergniolle, S., G. Brandeis, and J. C. Mareschal (1996), Strombolian explosions: 2. Eruption dynamics determined from acoustic measurements, *J. Geophys. Res.*, *101*, 20,449–20,466.

Wallis, G. B. (1969), *One-Dimensional Two-Phase Flow*, McGraw-Hill, New York.

White, E. T., and R. H. Beardmore (1962), The velocity of rise of single cylindrical air bubbles through liquids contained in vertical tubes, *Chem. Eng. Sci.*, *17*, 351–361.

B. A. Chouet, U.S. Geological Survey, 345 Middlefield Road, Menlo Park, CA 94025, USA.

M. R. James and S. J. Lane, Department of Environmental Science, Lancaster University, Lancaster LA1 4YQ, UK. (m.james@lancaster.ac.uk)